Personalized brain models identify neurotransmitter receptor changes in Alzheimer's disease

Ahmed Faraz Khan[1,2,3], Quadri Adewale[1,2,3], Tobias R. Baumeister[1,2,3], Felix Carbonell[4], Karl Zilles[5], Nicola Palomero-Gallagher[5,6,7,8], Yasser Iturria-Medina[1,2,3]*, for the Alzheimer's Disease Neuroimaging Initiative[9]

[1]Department of Neurology and Neurosurgery, Montreal Neurological Institute, McGill University, Montreal, Quebec, Canada

[2]McConnell Brain Imaging Center, Montreal Neurological Institute, Montreal, Canada

[3]Ludmer Centre for Neuroinformatics & Mental Health, Montreal, Canada

[4]Biospective Inc., Montreal, Canada

[5]Institute of Neuroscience and Medicine (INM-1), Research Centre Jülich, Jülich, Germany

[6]Cécile and Oskar Vogt Institute of Brain Research, Medical Faculty, Heinrich-Heine University, Düsseldorf, Germany

[7]Department of Psychiatry, Psychotherapy, and Psychosomatics, Medical Faculty, RWTH Aachen, Aachen, Germany

[8]JARA - Translational Brain Medicine, Aachen, Germany

[8]Data used in preparation of this article were partly obtained from the Alzheimer's Disease Neuroimaging Initiative (ADNI) database (adni.loni.usc.edu). As such, the investigators within the ADNI contributed to the design and implementation of ADNI and/or provided data but did not participate in analysis or writing of this report. A complete listing of ADNI investigators can be found at: http://adni.loni.usc.edu/wp-content/uploads/how_to_apply/ADNI_Acknowledgement_List.pdf

* Correspondence to: Y I-M, 3801 University Street, room NW312, Montreal Neurological Institute, McGill University, Montreal, Canada H3A 2B4. Email: iturria.medina@gmail.com

Abstract

Alzheimer's disease (AD) involves many neurobiological alterations from molecular to macroscopic spatial scales, but we currently lack integrative, mechanistic brain models characterizing how factors across different biological scales interact to cause clinical deterioration in a way that is subject-specific or personalized. Neurotransmitter receptors, as important signaling molecules and potential drug targets, are key mediators of interactions between many neurobiological processes altered in AD. We present a neurotransmitter receptor-enriched multifactorial brain model, which integrates spatial distribution patterns of 15 neurotransmitter receptors from *post-mortem* autoradiography with multiple *in-vivo* neuroimaging modalities (tau, amyloid-β and glucose PET, and structural, functional and arterial spin labeling MRI) in a personalized, generative, whole-brain formulation. Applying this data-driven model to a heterogeneous aged population (N=423, ADNI data), we observed that personalized receptor-neuroimaging interactions explained about 70% (± 20%) of the across-population variance in longitudinal changes to the six neuroimaging modalities, and up to 39.7% ($P<0.003$, FWE-corrected) of inter-individual variability in AD cognitive deterioration via an axis primarily affecting executive function. Notably, based on their contribution to the clinical severity in AD, we found significant functional alterations to glutamatergic interactions affecting tau accumulation and neural activity dysfunction, and GABAergic interactions concurrently affecting neural activity dysfunction, amyloid and tau distributions, as well as significant cholinergic receptor effects on tau accumulation. Overall, GABAergic alterations had the largest effect on cognitive impairment (particularly executive function) in our AD cohort (N=25). Furthermore, we demonstrate the clinical applicability of this approach by characterizing subjects based on individualized 'fingerprints' of receptor alterations. This study introduces the

first robust, data-driven framework for integrating several neurotransmitter receptors, multi-modal neuroimaging and clinical data in a flexible and interpretable brain model. It enables further understanding of the mechanistic neuropathological basis of neurodegenerative progression and heterogeneity, and constitutes a promising step towards implementing personalized, neurotransmitter-based treatments.

***Keywords*—** neurotransmitter receptors, multimodal neuroimaging, Alzheimer's disease, whole-brain computational model, personalized medicine.

***Running title*—**Receptors altered in Alzheimer's disease

***Abbreviations*—** AD = Alzheimer's disease; ADAS = Alzheimer's Disease Assessment Scale; ADNI = Alzheimer's Disease Neuroimaging Initiative; ASL = arterial spin labeling; CBF = cerebral blood flow; MCI = mild cognitive impairment; MMSE = Mini-Mental State Examination; PHS = polygenic hazard score; = re-MCM = receptor-enriched multifactorial causal model; ROI = region(s) of interest; SVD = singular value decomposition

Introduction

Alzheimer's disease (AD) involves degenerative changes to several neurobiological processes spanning molecular to macroscopic scales, including proteinopathies, modified gene expression, synaptic alterations, vascular dysregulation, hypometabolism, and structural atrophy [1]. In AD, these processes begin decades before the manifestation of cognitive deterioration [2], with vast inter-patient heterogeneity in age of disease onset, spatial distribution of neuropathologies, progression patterns, and clinical presentation [3]. Currently, there are no effective disease-modifying treatments for AD, despite many expensive attempts [2 3]. These failures may be attributed to: i) the use of a generalized medicine approach to treatment without considering the pathophysiological and clinical heterogeneity of the disease [4 5 6], ii) the focus on single disease factors (e.g. tau and amyloid) whereas most biological mechanisms in AD are multi-factorial [7], and, importantly, iii) an incomplete multi-scale understanding of how molecular and macroscopic factors interact to cause disease progression [8].

Recently, multi-modal neuroimaging models [9 10] have unravelled the temporal ordering of macroscopic structural, functional, vascular and proteinopathy changes in AD. Furthermore, personalized models of longitudinal neuroimaging data have been used to identify subject-specific alterations of neurobiological processes including tau and amyloid accumulation, blood flow, and neural activity at rest [11]. Nevertheless, such neuroimaging models lack a mechanistic basis in molecular and cellular processes. While these modalities may involve molecular imaging, such as amyloid or tau PET, their spatial resolution is limited in practice [12]. Identifying important pathways between truly microscopic-scale variables and observable macroscopic neuroimaging (i.e. molecular PET and MRI) in AD would both advance the understanding of the underlying biology and improve the selection of therapeutic targets tailored to an individual's particular disease subtype or presentation.

One particularly relevant class of molecules is neurotransmitter receptors, which regulate a variety of biological processes known to be dysfunctional in neurodegeneration. As neurotransmitter receptors are mediators of many relevant neurobiological factors, studying them is critical for a complete mechanistic understanding and the potential treatment of abnormal

brain conditions such as neurodegeneration [1]. For example, dopamine receptors expressed by the cerebral microvasculature and glial cells appear to modulate the coupling between neural activity and vascular response [13], which is altered in AD [14]. As an organ, the brain consumes energy disproportionately to its mass [15]. A significant fraction of this energy expenditure is attributed to synaptic signalling and molecular synthesis, with approximately 37% of this associated with postsynaptic receptors and housekeeping processes [16]. The production and degradation of neurotransmitter receptors is a complex, dynamic process that is regulated in response to changes in many variables, such as receptor activation, gene expression, and external stimuli [17]. Since these processes are energy-intensive, changes to their concentrations are likely to indicate relevant biological alterations, making them a potential therapeutic target. Although it is not primarily considered a neurotransmitter disease, AD is associated with dysfunction in several important neurotransmitter receptor systems. Particularly, acetylcholine and glutamate receptors are implicated in essential stages of a pathological neurodegenerative cascade, including cholinergic hydrolysis and glutamatergic excitotoxicity [1]. Neurotransmitter receptor alterations are also suspected of being a mechanistic pathway in healthy ageing [18]. Thus, integrating neurotransmitter receptors with macroscopic neuroimaging data has the potential to uncover molecular pathways important to ageing and disease progression. However, *in-vivo* neurotransmitter receptor imaging is difficult, due to the lack of specific *in-vivo* radiolabels [19]. Typically, receptor mapping has involved either post-mortem histology, or expensive positron emission tomography (PET) imaging for a limited set of molecules with available radionuclides. As such, large longitudinal *in-vivo* datasets for several receptors would be extremely expensive or technologically infeasible to collect. Consequently, alterations to neurotransmitter systems during disease progression are not well characterized [20].

Motivated by these concerns, we propose a whole-brain generative formulation integrating high resolution *in vitro* neurotransmitter receptor density maps and *in vivo* multi-modal neuroimaging. For the first time, this model allows a quantitative comparison of the causal role of different neurotransmitter receptors and neuroimaging modalities in healthy aging and neurodegeneration. Specifically, we fit subject-specific generative models of neuroimaging data in an aging population covering the AD spectrum (N=423, ADNI data), augmented with 15 whole-brain neurotransmitter receptor distribution patterns. We then treat the parameters of these personalized models as subject-specific measures representing latent receptor-neuroimaging interactions, and identify multi-scale interactions that explain mechanistic variability and cognitive heterogeneity between AD subjects. We find that receptor density maps and their interactions with neuroimaging significantly improve the fit of neuroimaging models, providing a valid proxy for true, longitudinal *in-vivo* receptor imaging. Examining model parameters in AD patients, we found an axis of variability between receptor-imaging interactions and cognitive decline, primarily affecting executive function. Specifically, this axis is influenced by predictors of tau distribution and resting state neural activity, concordant with recent reports in late-onset AD [21 22]. Via this axis, mechanisms of glutamatergic, cholinergic and GABAergic receptor interactions correlated significantly with cognitive decline in AD. In contrast, while receptor-imaging interactions in healthy individuals did not vary significantly with cognitive status, mechanisms affecting cerebral blood flow (CBF) changes and gray matter atrophy accounted for most of the inter-individual heterogeneity. This work represents the earliest attempt to integrate several neurotransmitter receptors and multi-modal neuroimaging data in a universal formulation, representing a notable advance towards implementing individually-tailored neurotransmitter-based diagnosis and treatment in neurodegeneration.

Materials and Methods

Ethics Statement

The study was conducted according to Good Clinical Practice guidelines, the Declaration of Helsinki, US 21CFR Part 50–Protection of Human Subjects, and Part 56–Institutional Review Boards, and pursuant to state and federal HIPAA regulations (adni.loni.usc.edu). Study subjects and/or authorized representatives gave written informed consent at the time of enrollment for sample collection and completed questionnaires approved by each participating site Institutional Review Board (IRB). The authors obtained approval from the ADNI Data Sharing and Publications Committee for data use and publication, see documents http://adni.loni.usc.edu/wp-content/uploads/how_to_apply/ADNI_Data_Use_Agreement.pdf and http://adni.loni.usc.edu/wp-content/uploads/how_to_apply/ADNI_Manuscript_Citations.pdf, respectively.

Data description and processing

Study participants

This study used longitudinal data from N=423 participants (149 healthy, 151 early mild cognitive impairment (EMCI), 103 late mild cognitive impairment (LMCI), and 20 AD-diagnosed subjects at baseline) from the Alzheimer's Disease Neuroimaging Initiative (ADNI) (adni.loni.usc.edu). Demographic information is summarized in Supplementary Table S1. At least three different imaging modalities were acquired for each included subject (i.e. structural MRI, fluorodeoxyglucose PET, resting functional MRI, Arterial Spin Labeling and/or Amyloid-ß PET). The ADNI was launched in 2003 as a public-private partnership, led by Principal Investigator Michael W. Weiner, MD. The primary goal of ADNI has been to test whether serial magnetic resonance imaging (MRI), PET, other biological markers, and clinical and neuropsychological assessments can be combined to measure the progression of mild cognitive impairment (MCI) and early Alzheimer's disease (AD).

Structural MRI acquisition/processing

Brain structural T1-weighted 3D images were acquired for all N=423 subjects. For a detailed description of acquisition details, see http://adni.loni.usc.edu/methods/documents/mri-protocols/. All images underwent non-uniformity correction using the N3 algorithm [23]. Next, they were segmented into grey matter, white matter and cerebrospinal fluid (CSF) probabilistic maps, using SPM12 (fil.ion.ucl.ac.uk/spm). Grey matter segmentations were standardized to MNI space [24] using the DARTEL tool [25]. Each map was modulated in order to preserve the total amount of signal/tissue. Mean grey matter density and determinant of the Jacobian (DJ) [25] values were calculated for the regions described in *Methods: Data description and processing: Receptor densities and brain parcellation.* For each region, obtained grey matter density and DJ values were statistically controlled for differences in acquisition protocols. Both measurements provided equivalent modeling results. All the results/figures presented in this study correspond to the DJ, which constitutes a robust local measure of structural atrophy.

Fluorodeoxyglucose PET acquisition/processing

A 185 MBq (5 ± 0.5 mCi) of [18F]-FDG was administered to each participant (N=418) and brain PET imaging data were acquired approximately 20 min post-injection. All images were corrected using measured attenuation. Also, images were preprocessed according to four main steps [26]: 1) dynamic co-registration (separate frames were co-registered to one another lessening the effects of patient motion), 2) across time averaging, 3) re-sampling and reorientation from native space to a standard voxel image grid space ("AC-PC" space), 4) spatial filtering to produce images of a uniform isotropic resolution of 8 mm FWHM, and 5) affine registration to the participant's structural T1 image. Next, using the registration parameters obtained for the structural T1 image with nearest acquisition date, all FDG-PET images were spatially normalized to the MNI space [24]. Regional standardized uptake value ratio (SUVR) values for the regions considered were calculated using the cerebellum as reference region.

Resting fMRI acquisition/processing

Resting-state functional images were obtained using an echo-planar imaging sequence on a 3.0-Tesla Philips MRI scanner for N=127 subjects. Acquisition parameters were: 140 time points, repetition time (TR)=3000 ms, echo time (TE)=30 ms, flip angle=80°, number of slices=48, slice thickness=3.3 mm, in plane resolution=3 mm and in plane matrix=64×64. Pre-processing steps included: 1) motion correction, 2) slice timing correction, 3) alignment to the structural T1 image, and 4) spatial normalization to MNI space using the registration parameters obtained for the structural T1 image with the nearest acquisition date, and 5) signal filtering to keep only low frequency fluctuations (0.01–0.08 Hz) [27]. For each brain region, our model requires a local (i.e. intra-regional, non-network) measure of functional activity, in order to maintain mechanistic interpretability and to prevent data leakage of network information into local model terms (described further in *Receptor-Enriched Multifactorial Causal Model*). Due to its high correlation with glucose metabolism [28] and validation as an AD-sensitive metric [29] [30], we calculated regional fractional amplitude of low-frequency fluctuation (fALFF) [31] as a measure of functional integrity.

Furthermore, while our model uses structural connectivity as the network along which inter-region propagation occurs, we also calculated and used a functional connectome, as the average of the absolute Pearson correlation matrices across all healthy subjects with fMRI data (N=42). Based on this, we compared model performance using structural and functional connectivity, characterizing the choice of connectivity metrics (see *Multi-scale interactions involving neurotransmitter receptors are important to explaining multifactorial brain reorganization* and Supplementary Fig. S8).

ASL acquisition/processing

Resting Arterial Spin Labeling (ASL) data were acquired using the Siemens product PICORE sequence for N=195 subjects. Acquisition parameters were: TR/TE=3400/12 ms, TI1/TI2=700/1900 ms, FOV=256 mm, 24 sequential 4 mm thick slices with a 25% gap between the adjacent slices, partial Fourier factor=6/8, bandwidth=2368 Hz/pix, and imaging matrix=64×64. For preprocessing details see "UCSF ASL Perfusion Processing Methods" in adni.loni.usc.edu. In summary, main preprocessing steps included: 1) motion correction, 2) perfusion-weighted images (PWI) computation, 3) intensity scaling, 4) CBF images calculation,

5) alignment to the structural T1 image, and 6) spatial normalization to MNI space [24] using the registration parameters obtained for the structural T1 image with the nearest acquisition date, and 6) mean CBF calculation for each considered brain region.

Amyloid-ß PET acquisition/processing

A 370 MBq (10 mCi ± 10%) bolus injection of AV-45 was administered to each participant (N=422), and 20 min continuous brain PET imaging scans were acquired approximately 50 min post-injection. The images were reconstructed immediately after the 20 min scan, and when motion artifact was detected, another 20 min continuous scan was acquired. For each individual PET acquisition, images were initially preprocessed according to four main steps [26]: 1) dynamic co-registration (separate frames were co-registered to one another lessening the effects of patient motion), 2) across time averaging, 3) re-sampling and reorientation from native space to a standard voxel image grid space ("AC-PC" space), 4) spatial filtering to produce images of a uniform isotropic resolution of 8 mm FWHM, and 5) affine registration to the participant's structural T1 image. Next, using the registration parameters obtained for the structural T1 image with the nearest acquisition date, all amyloid images were spatially normalized to the MNI space [24]. Considering the cerebellum as an Aß non-specific binding reference, SUVR values for the regions were calculated.

Tau PET acquisition/processing

A 370 MBq/kg bolus injection of tau specific ligand 18F-AV-1451 ([F- 18] T807) was administered to each participant (N=238), and 30 min (6 × 5 min frames) brain PET imaging scans were acquired starting at 75 min post-injection (N = 200). Images were preprocessed according to four main steps [26]: 1) dynamic co-registration (separate frames were co-registered to one another lessening the effects of patient motion), 2) across time averaging, 3) re-sampling and reorientation from native space to a standard voxel image grid space ("AC-PC" space), 4) spatial filtering to produce images of a uniform isotropic resolution of 8mm FWHM, and 5) affine registration to the participant's structural T1 image. Next, using the registration parameters obtained for the structural T1 image with the nearest acquisition date, all tau images were spatially normalized to the MNI space [24]. Considering the cerebellum as a non-specific binding reference, SUVR values for the grey matter regions considered were calculated.

Receptor densities and brain parcellation

In-vitro quantitative receptor autoradiography was applied to measure the densities of 15 receptors in 44 cytoarchitectonically defined cortical areas spread throughout the brain [32]. These receptors span major neurotransmitter systems, and show significant regional variability across the brain. Brains were obtained through the body donor programme of the University of Düsseldorf. Donors (three male and one female; between 67 and 77 years of age) had no history of neurological or psychiatric diseases, or long-term drug treatments. Causes of death were non-neurological in each case. Each hemisphere was sliced into 3 cm slabs, shock frozen at -40C, and stored at -80C.

Receptors for the neurotransmitters glutamate (AMPA, NMDA, kainate), GABA ($GABA_A$, $GABA_A$-associated benzodiazepine binding sites, $GABA_B$), acetylcholine (muscarinic M_1, M_2, M_3, nicotinic $\alpha_4\beta_2$), noradrenaline (α_1, α_2), serotonin ($5\text{-}HT1_A$, $5\text{-}HT_2$), and dopamine (D_1) were labeled according to previously published binding protocols consisting of pre-incubation, main

incubation and rinsing steps 32. The ligands used are summarized in Supplementary Table S3. Receptor densities were quantified by densitometric analysis of the ensuing autoradiographs, and areas were identified by cytoarchitectonic analysis in sections neigbouring those processed for receptor autoradiography, and which had been used for the visualization of cell bodies [33].

A brain parcellation was then defined with the aid of the Anatomy Toolbox [34] using 44 regions of interest for which receptor densities were available 35. This parcellation was based on areas identified by cortical cytoarchitecture, as well as other cyto- and receptor-architectonically defined regions with receptor measurements (regions are summarized in Supplementary Table S4). These 44 regions were mirrored across left and right hemispheres for a total of 88 brain regions in our parcellation. For each receptor, regional densities were normalized using the mean and standard deviation across all 88 brain regions.

The structural T1 images of the Jülich [34] and Brodmann [36] brain parcellations were registered to the MNI ICBM152 T1 template using FSL 5.0's FLIRT affine registration tool [37], and the obtained transformations were used to project the corresponding parcellations to the MNI ICBM152 space (using nearest neighbor interpolation to conserve original parcellation values). In the MNI ICBM152 space, voxels corresponding to the cytoarchitectonically-defined regions from [35] were identified from the regions in the Anatomy Toolbox, with the remaining Brodmann regions (Supplementary Table S4) filled in using the Brodmann brain atlas. The resulting parcellation of 88 brain regions in the common template space was then used to extract whole-brain multi-modal neuroimaging data and estimate the diffusion-based connectivity matrix, as described in *Materials and Methods: Multimodal neuroimaging data and Materials and Methods: Anatomical connectivity estimation.*

Anatomical connectivity estimation

The connectivity matrix was constructed using DSI Studio (http://dsi-studio.labsolver.org). A group average template was constructed from a total of 1065 subjects [38]. A multishell diffusion scheme was used, and the b-values were 990, 1985 and 2980 s/mm2. The number of diffusion sampling directions were 90, 90, and 90, respectively. The in-plane resolution was 1.25 mm. The slice thickness was 1.25 mm. The diffusion data were reconstructed in the MNI space using q-space diffeomorphic reconstruction [39] to obtain the spin distribution function [40]. A diffusion sampling length ratio of 2.5 was used, and the output resolution was 1 mm. The restricted diffusion was quantified using restricted diffusion imaging [41]. A deterministic fiber tracking algorithm [42] was used. A seeding region was placed at whole brain. The QA threshold was 0.159581. The angular threshold was randomly selected from 15 degrees to 90 degrees. The step size was randomly selected from 0.5 voxel to 1.5 voxels. The fiber trajectories were smoothed by averaging the propagation direction with a percentage of the previous direction. The percentage was randomly selected from 0% to 95%. Tracks with length shorter than 30 or longer than 300 mm were discarded. A total of 100000 tracts were calculated. A custom brain atlas based on cytoarchitectonic regions with neurotransmitter receptor data [35] was used as the brain parcellation, as described in *Materials and Methods*: *Data description and processing: Receptor densities and brain parcellation*, and the connectivity matrix was calculated by using count of the connecting tracks.

Multimodal neuroimaging data

After pre-processing ADNI neuroimaging data for all 6 modalities and extracting it for the cytoarchitectonically defined atlas described in *Materials and Methods: Data description and processing: Receptor densities and brain parcellation*, subjects lacking sufficient longitudinal or multimodal data were discarded. The disqualification criteria were i) fewer than 4 imaging modalities with data, or ii) fewer than 3 longitudinal samples for all modalities. For the remaining subjects, missing neuroimaging modalities at each time point with actual individual data were imputed using trimmed scores regression with internal PCA [43]. Imputation accuracy was validated using 10-fold cross-validation, showing a strong capacity to recover the real data (correlation values: $r_{CBF} = 0.44$, $r_{amyloid} = 0.60$, $r_{neural\ activity} = 0.95$, $r_{gray\ matter} = 0.80$, $r_{metabolism} = 0.81$, $r_{tau} = 0.71$; all $P<10^{-6}$). Finally, a total of 423 subjects were left with all 6 neuroimaging modalities with an average of 4.75 (±2.71) time points. We used the mean and variance of each neuroimaging modality across all regions and healthy subjects to calculate z-scores of neuroimaging data across all (healthy, MCI, and AD) subjects. Please see Supplementary Tables S1-S2 for demographic characteristics, and *Materials and Methods: Multimodal neuroimaging data* and Supplementary Fig. S1 for a detailed flowchart of the selection and analysis of the participants.

Cognitive scores

We used multiple composite scores derived from the ADNI neuropsychological battery. Protocols for deriving each score are described in the respective ADNI protocols documentation or relevant publication for executive function 44, memory 44, language [45], visuospatial functioning [45], mini-mental state examination (MMSE) [46], and the Alzheimer's Disease Assessment Scale (ADAS11/13) 46. With an average of 7.27 ± (2.55) evaluations per subject in our cohort (N=423), we calculated cognitive decline as the linear best fit rate of change of each cognitive score with respect to examination date. Thus, for each patient, cognitive decline was represented by a set of 7 rates of change.

Receptor-Enriched Multifactorial Causal Model (re-MCM)

Under the framework of the multifactorial causal model (MCM) introduced in [11], we consider the brain as a dynamical system of anatomically-connected regions defined by interacting, neuroimaging-derived biological factors. These biological factors are tissue structure, neuronal activity, blood flow, metabolism, and the accumulation of misfolded proteins (amyloid, tau), quantified by structural MRI, functional MRI, ASL MRI, FDG PET, amyloid PET and tau PET, respectively. Each biological factor m at a particular brain region i is represented by a single variable $S_{m,i}$, whose rate of change is a function of i) local states of other factors, and ii) the propagation of the same factor across anatomically-connected regions. Thus, in our model, pathological factors can propagate throughout the brain, but any direct interactions between factors must occur locally within a region.

In this study, for a given subject, and at each of the $N_{\mathrm{ROI}} = 88$ brain regions, the system is defined by $N_{\mathrm{fac}} = 6$ state variables or factors. Each factor $S_{m,i}$ represents the m^{th} neuroimaging modality at the i^{th} brain region. Factor dynamics can be decomposed into local effects due to factor-factor interactions and network propagation of the factor. In general, the differential equation describing this coupled system for a given subject is:

$$\frac{dS_{m,i}(t)}{dt} = \underbrace{f(\mathbf{S}_{*,i}(t))}_{\text{Local Effects}} + \underbrace{g(\mathbf{S}_{m,*}(t), C_{i\leftrightarrow *})}_{\text{Inter-region Propagation}}, \quad (1)$$

where f and g are functions that determine the effects of local multi-modal interactions and propagation, respectively, and $C_{i\leftrightarrow *}$ is the net connectivity of region i. Here, we extend the basic MCM formulation (Equation 1) to include the local effects of neurotransmitter receptors. With **R** being a $N_{\text{rec}} \times N_{\text{ROI}}$ matrix of spatial maps, composed of local densities $r_{k,i}$ of a receptor k at a region i, and $\mathbf{R}_{*,i}$ being a $N_{\text{rec}} \times 1$ vector of all receptor densities in region i, we define the general form of the receptor-enriched MCM (re-MCM) as:

$$\frac{dS_{m,i}(t)}{dt} = f(\mathbf{S}_{*,i}(t), \mathbf{R}_{*,i}) + g(\mathbf{S}_{m,*}(t), C_{i\leftrightarrow *}). \quad (2)$$

The first term $f(\mathbf{S}_{*,i}(t), \mathbf{R}_{*,i})$ represents the local component, which is the interaction between the factor m and all other factors in region i, mediated by the local densities of receptors in that region. The second term $g(\mathbf{S}_{m,*}(t), C_{i\leftrightarrow *})$ represents the contribution due to network propagation of the factor m, mediated by the net anatomical connectivity $C_{i\leftrightarrow *}$ of the region i. The functions f and g in Equation 2 define the global imaging factor dynamics, which are valid for all brain regions. Thus, regional differences are due to different imaging factor states, receptor distributions and anatomical connectivity, but the mechanisms of their interactions, represented by f and g, are consistent across the whole brain.

Given the decades-long temporal scale of neurodegeneration compared to the relatively short few months between neuroimaging samples, we assume a locally linear, time-invariant dynamical system:

$$\frac{dS_i^m(t)}{dt} = \sum_{n=1}^{N_{\text{fac}}} \alpha^{n\to m} S_{n,i}(t) + \sum_{k=1}^{N_{\text{rec}}} \alpha_k^m r_{k,i} + \alpha_{\text{prop}}^m \sum_{j=1, j\neq i}^{N_{\text{ROI}}} \left[C_{j\to i} S_{m,j}(t) - C_{i\to j} S_{m,i}(t)\right], \quad (3)$$

where $C_{i\to j}$ is the directed anatomical connectivity from region i to j, and $\frac{dS_{m,i}(t)}{dt}$ was defined by the local rate of change of neuroimaging data for successive longitudinal samples at times t' and t:

$$\frac{dS_{m,i}(t)}{dt} = \frac{S_{m,i}(t) - S_{m,i}(t')}{t - t'}. \quad (4)$$

In this work, we expand the local effect term to include i) direct factor-factor effects, ii) interaction terms mediated by $N_{\text{rec}} = 15$ receptor types, and iii) direct receptor effects (Equation 3) on the neuroimaging factor rate of change $\frac{dS_{m,i}}{dt}$. The local factor effects term n Equation 3 is now expanded:

$$\alpha^{n\to m} = \underbrace{\alpha_0^{n\to m}}_{\text{Direct Factor-Factor Term}} + \underbrace{\sum_k^{N_{\text{rec}}} \alpha_k^{n\to m} r_i^k}_{\text{Interaction Term}}. \quad (5)$$

Although the receptor maps **R** are constant templates with spatial but no temporal variation, their interaction terms add a dynamic element, as they imply a regional heterogeneity to neuroimaging predictors that is not directly explained by the direct receptor term in Equation 3. For instance, we might notice that (hypothetically) the interaction between a glutamatergic receptor and functional activity is a significant predictor of gray matter atrophy. Whether or not functional activity or the glutamatergic receptor map are significant predictors on their own, the

significance of the interaction term would imply that the spatial distribution template of the glutamatergic receptor is informative when combined with functional activity.

Additionally, for propagation, we consider only symmetric connectivity $C_{j\leftrightarrow i}$ between regions i and j, using a template connectivity matrix for all subjects, as described in *Anatomical connectivity estimation*, to give the propagation term

$$p_{m,i}(t) = \sum_{j=1,j\neq i}^{N_{\text{ROI}}} C_{j\leftrightarrow i}\left[S_{m,j}(t) - S_{m,i}(t)\right]. \quad (6)$$

This reduces the net propagation of a factor m to a region i to a single propagation term. A more complete treatment may consider vascular connectivity as well [11] 4, as this measure may be more relevant for different processes (such as functional activity, CBF and metabolism, respectively).

$$\frac{dS_{m,i}(t)}{dt} = \sum_{n=1}^{N_{\text{fac}}}\left(\alpha_0^{n\to m} + \sum_k^{N_{\text{rec}}} \alpha_k^{n\to m}\, r_{k,j}\right) S_{n,i}(t) + \sum_{k=1}^{N_{\text{rec}}} \alpha_k^m\, r_{k,i} + \alpha_{\text{prop}}^m p_{m,i}(t) \quad (7)$$

Formulated in this way, each model contains a set of $N_{\text{params}} = N_{\text{fac}} \times (1 + N_{\text{rec}}) + N_{\text{rec}} + 1 = 113$ parameters $\{\alpha\}_x^m$ for subject x and factor m (or 678 total parameters per subject). Apart from the propagation term, which is specific to the imaging modality output of the model, all predictors are identical for the 6 neuroimaging modalities. That is, a common set of receptor maps, multi-modal neuroimaging states, and pseudo-personalized receptor-imaging interactions are used as predictors. However, based on their respective effects on each output modality, we obtain 678 distinct biological parameters per subject, each with a distinct mechanistic interpretation (e.g. the effect of neural activity on metabolism or the effect of neural activity on CBF). We then perform linear regression, using the terms in Equation 7 as predictors with longitudinal ADNI neuroimaging samples $S_{m,i}(t)$ and receptor maps **R**, to estimate subject- and modality-specific parameters $\{\alpha\}_x^m$ for each subject x and modality m. Separate regression models were built for i) each of the N=423 qualifying subjects, and ii) each of the 6 neuroimaging factors. These subjects were drawn from the ADNI dataset with at least 4 recorded neuroimaging modalities, and at least 3 longitudinal samples for at least one modality.

To evaluate model fit, we calculate the coefficient of determination (R^2) for each subject. This is summarized by modalities in Fig. 2. With the data vector $\mathbf{y}$ with elements $y_{m,i,t} = \frac{dS_{m,i}(t)}{dt}$, and model predictions $\hat{\mathbf{y}}$ with $\hat{y} = \hat{y}_{m,i,t}$, the coefficient of determination is

$$R^2 = 1 - \frac{\sum_{i,t}(\mathbf{y}_{m,i,t} - \hat{\mathbf{y}}_{m,i,t})^2}{\sum_{i,t}(\mathbf{y}_{m,i,t} - <\mathbf{y}_m>)^2}, \quad (8)$$

where $<\mathbf{y}_m>$ is the mean of neuroimaging data for a particular modality m across all brain regions and longitudinal samples.

Statistical analysis

Model fit

Personalized model fit quantified by the coefficient of determination (R^2) was evaluated for each subject and neuroimaging modality. F-tests were used to compare receptor-neuroimaging (113 parameters per modality) and neuroimaging-only (8 parameters per modality) to fitting

neuroimaging data in each subject (F-test with $p<0.05$). The model fit (R^2) was evaluated for each subjects' neuroimaging models using 1000 iterations of randomly permuted receptor maps (with receptor densities shuffled across regions independently for each receptor type), and we calculated the p-value of the true receptor data model R^2 compared to this distribution.

Biological parameters and relationship with cognition

We aimed to further clarify how the cognitive decline observed in AD progression is modulated by specific neurotransmitter receptor systems and their causal interactions with macroscopic biological factors (i.e. amyloid, tau, CBF, neural activity, glucose metabolism and gray matter density). As changes in several receptor densities are difficult to image *in-vivo*, we analyzed the receptor terms from our personalized re-MCM approach as a proxy for the importance of each particular receptor's distribution or interactions in predicting multi-domain cognitive deterioration in AD. To consider the inter-subject variability in the diseased population, we used a combination of cognitive assessment scores as disease severity descriptors (i.e. executive function, memory, language, visuospatial functioning, MMSE, ADAS 11 and ADAS 13; see *Materials and Methods*: *Cognitive Scores*).

We aimed to robustly identify significant and relevant re-MCM parameters that represent molecular-neuroimaging interactions associated with cognitive decline, using a data-driven multivariate cross-correlation analysis in combination with a randomized permutation test to ensure the statistical stability of our results. By concurrently analyzing the multivariate changes across all re-MCM parameters, this multidimensional analysis searched for large clusters of functionally related receptor-neuroimaging interaction mechanisms statistically associated with AD-associated cognitive changes. In other words, the SVD method used here (and its associated permutation test) identified the specific set of receptors and/or imaging features that were maximally related to cognitive decline. To this end, we selected a clinical subgroup of interest (either N=112 cognitively healthy subjects or N=25 AD patients from the N=423 total subjects with sufficient multi-modal neuroimaging data), and performed the following procedure on the original set of 678 re-MCM parameters and 7 rates of cognitive decline per subject (executive function, memory, language, visuospatial functioning, MMSE, and ADAS11/13):

1. To identify correlated axes of variation, we performed principal component analysis (PCA) on all 678 biological parameters separately on the healthy and AD subjects, and ranked parameters based on the variance explained in the first principal component (PC).

2. To relate biological parameters to cognition, we performed singular value decomposition (SVD) on the cross-covariance matrix between significant parameters and rates of cognitive decline for AD patients, after adjusting for covariates (baseline age, education and gender). SVD allows us to simultaneously reduce the dimensionality of the 7 cognitive assessments and to rank parameters by their variation with cognition. Where X is a matrix of z-scores of each re-MCM parameter for this clinical subgroup and Y is a matrix of the corresponding z-scores of the rates of clinical decline, the cross-covariance matrix $C = XY'$ is decomposed as

   $$C = USV' \tag{9}$$

   where U and V are orthonormal matrices of spatial loadings for the coefficients and cognitive scores, respectively, and S is a (diagonal) matrix of singular values $\{s_1, \dots, s_7\}$.

3. To evaluate the significance of SVD components, we performed permutation tests by shuffling the mapping between subjects' re-MCM parameters and cognitive scores, and repeating SVD. To compare permuted iterations, we performed a Procrustes transformation to align the axes of singular components. We kept only those singular components that are significant $p < 0.05$) compared to 1000 permutation iterations of SVD components.

4. We performed 1000 iterations of bootstrapping on the parameters X, and discarded the parameters with non-significant 95% confidence intervals.

5. For the remaining significant re-MCM parameters and SVD components, we computed the variance explained per parameter. We then summed the contribution of each significant parameter j to each significant SVD component i, weighted by the fraction of total variance explained by the i^{th} component

$$r_j^{2,\text{param,sig}} = \sum_i^{N_{\text{SVD,sig}}} \underbrace{\frac{U_{i,j}^2}{\sum_j U_{i,j}^2}}_{\substack{\text{Parameter} \\ \text{contribution}}} \underbrace{\frac{s_i^2}{\sum_j s_j^2}}_{\substack{\text{Singular value} \\ \text{contribution}}}. \quad (10)$$

Inter-subject mechanistic variability

To explore the potential clinical utility of our approach at the personalized level, we performed a quantitative comparison between diseased participants in terms of their inter-subject variability across different receptor systems. To this end, we defined individual-specific "fingerprints" of the alterations in receptor-modulated synergistic interactions. Specifically, for each participant *i* and receptor system *r*, we calculated the Mahalanobis distance $D_{i,r}$of re-MCM parameters $\alpha_{i,r}$ associated with cognitive decline in our AD cohort (Fig. 4; Supplementary Table S5). This distance is calculated between subject's parameters $\alpha_{i,r}$, and the distribution of healthy subjects' parameters for receptor *r*, with means $\mu_{i,r}$ and a covariate matrix $\boldsymbol{S^{-1}}$,

$$D_{i,r} = \sqrt{(\alpha_{i,r} - \mu_{i,r})^T \boldsymbol{S^{-1}} (\alpha_{i,r} - \mu_{i,r})}. \quad (11)$$

To quantify the relationship between this summary metric of receptor alterations and specific cognitive domains, we performed multivariate linear regression on rates of cognitive decline (adjusted by age, gender, education level and APOE4 status; N=25) using the z-scores of the Mahalanobis distances for the 6 receptor systems. We also estimated the explanatory importance of each receptor system, as the percentage improvement in model fit (R^2) by including a particular receptor Mahalanobis distance.

Data and code availability

The three datasets used in this study are available from the ADNI database (neuroimaging and cognitive evaluations; http://www.adni.loni.usc.edu), the HCP database (tractography template for connectivity estimation; http://www.humanconnectomeproject.org/), and receptor density data published in 35. We anticipate that the re-MCM method will be released soon as part of our available and open-access, user-friendly software 47 (https://www.neuropm-lab.com/neuropm-box.html).

Results

Capturing receptor-mediated multifactorial brain reorganization

Here, we aimed to develop a multi-scale generative brain model linking regional receptor densities (for 15 neurotransmitter receptors) and multimodal neuroimaging-based factors (for six biological variables) in a flexible, unified formulation. We aimed to use this mathematical framework to infer receptor alterations associated with the long-term physiological changes of complex brain reorganization processes (namely aging and neurodegeneration) and their cognitive impact. Because changes in receptor concentrations are difficult to measure *in vivo*, our receptor density maps were composed of group-averaged templates, with spatial distributions of receptors but no inter-individual variability or intra-individual longitudinal progression. Consequently, we use the predictive importance of receptor distributions in generative models of abnormal neuroimaging-derived biological variables as a proxy for alterations in either receptor density or mechanistic interactions with other imaging-derived variables.

We proceeded to characterize the multifactorial brain dynamics of each participant using the developed *neurotransmitter receptor-enriched multifactorial causal model* (re-MCM; Fig. 1) and the quality-controlled, multi-modal longitudinal neuroimaging data (described in *Materials and Methods: Data description and processing*). For each participant with sufficient longitudinal and multi-modal data (N=423), the re-MCM was fit for all 6 neuroimaging modalities, to obtain receptor-imaging biological parameters reflecting local factor-factor interactions mediated by neurotransmitter receptor distributions (e.g. amyloid-tau interactions modulated by NMDA receptors) and the spreading of effects via anatomical networks (e.g. amyloid and tau propagation along white matter connections).

a) Individual-level longitudinal multi-modal neuroimaging modeling

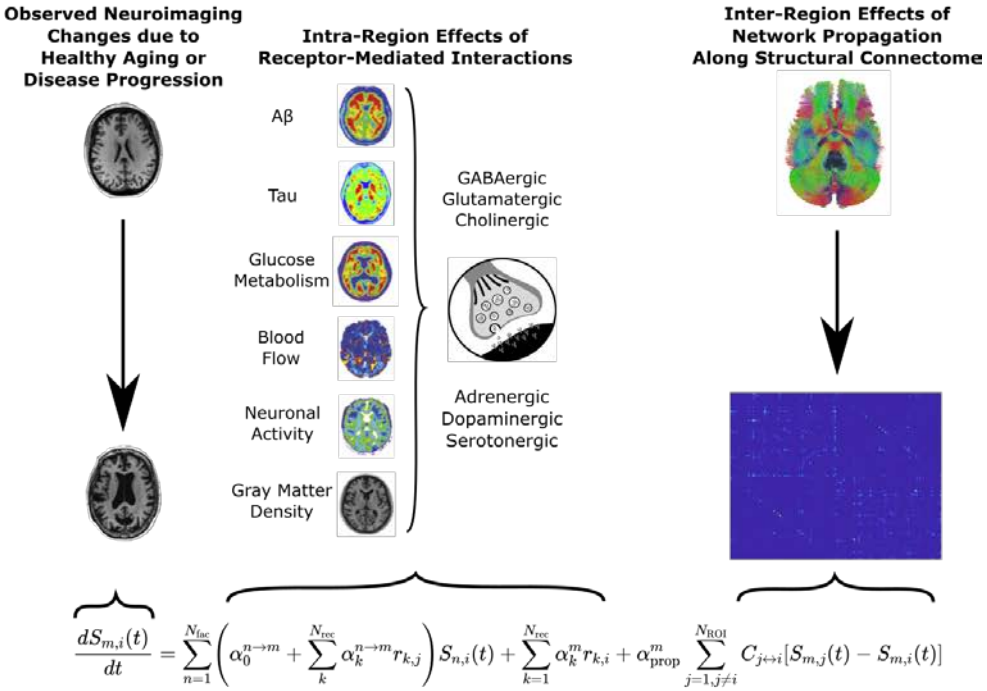

b) Population-level analysis to identify relevant biological parameters

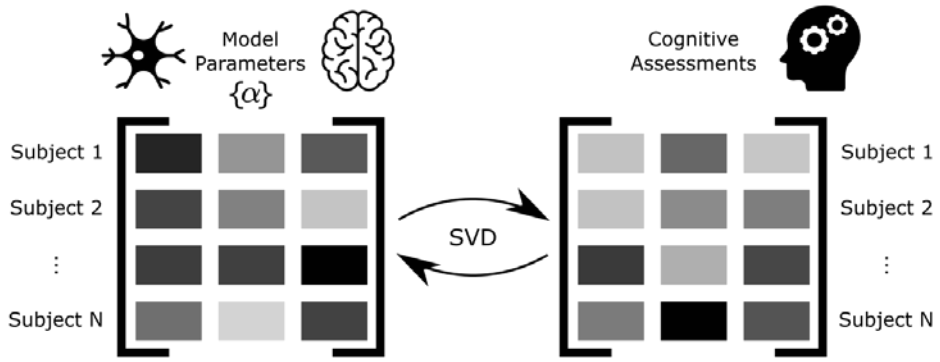

c) Personalized interventions based on specific mechanistic alterations

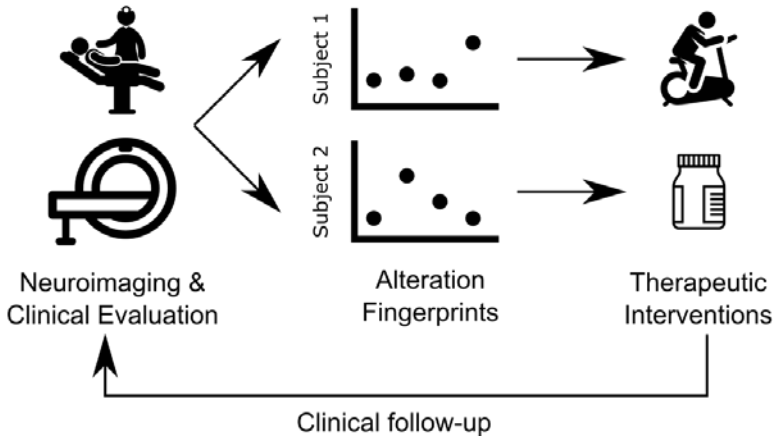

Figure 1: **Neurotransmitter receptor-enriched multifactorial causal modeling. a)** For each subject with longitudinal neuroimaging data, changes between subsequent samples in each neuroimaging modality are decomposed into local synergistic effects due to i) the direct influence of all neuroimaging-quantified biological factors, ii) receptor density distributions, and iii) multi-scale receptor-imaging interactions, and iv) global network-mediated intra-brain propagation. Combining this data across (N_{ROI}=88) brain regions and multiple neuroimaging samples results in a multivariate regression problem to identify the subject-specific parameters $\{\alpha\}$. **b)** At a group level, these personalized model parameters are then compared to subjects' cognitive assessments (specifically, the rates of decline for 7 composite cognitive scores described in *Materials and Methods: Cognitive scores*) using a singular value decomposition (SVD) procedure on the cross-covariance matrix, to identify multi-scale receptor-neuroimaging interactions that are robustly correlated with the severity of cognitive symptoms in AD (outlined in *Materials and Methods: Biological parameters and relationship with cognition)*. **c)** In the context of personalized applications, inter-subject variability in receptor-imaging interactions can be used as clinical "fingerprints" of molecular alterations representing different disease mechanisms. Patients can then receive individually-tailored treatment plans to address their underlying etiology, based on their specific fingerprints. For example, patients with greater vascular alterations may benefit more from lifestyle interventions such as physical exercise, whereas patients with greater receptor alterations may require neurotransmitter-based medication (depending on the most affected receptor). Furthermore, treatment plans can be continually adjusted with follow-up visits.

Multi-scale interactions involving neurotransmitter receptors are important to explaining multifactorial brain reorganization

Firstly, we proceeded to evaluate the ability of the re-MCM approach to fit longitudinal neuroimaging data with and without receptor maps and multi-scale receptors-imaging interactions (Fig. 2a-b). For each of the six neuroimaging modalities per subject, we calculated the coefficient of determination (R^2) as a measure of model accuracy for explaining the real imaging-specific longitudinal changes. While model accuracy varied by imaging modality, we observed that the personalized models including receptor-neuroimaging interactions explained approximately 70% ($\pm$ 20%) of observed variance in all modalities (Fig. 2a).

Inter-region propagation in our model occurs along structural connectivity. While functional connectivity can be a better predictor of fMRI data, structural connectivity is a better measure of the actual physical substrate connecting brain regions. Nevertheless, to explore the effects of alternate connectivity measures, we repeated our modeling steps using functional connectivity in place of the structural connectivity derived from diffusion-MRI tractography. While the connectivity matrices differed, we found almost no change in model fit or parameters across subjects, with a high correlation $r>0.99$ of model R^2 ($P<0.001$) across all modalities (Supplementary Fig. S8). We attribute this to the dominance of intra-regional effects in our model, with many interacting local receptor and neuroimaging predictors, and also to the shared information in structural and functional connectivity [48].

Next, to evaluate the relevance of receptor densities and receptor-mediated interactions between biological factors quantified by imaging (e.g. amyloid-tau interaction modulated by GABA), we compared the model fit of full re-MCM models (incorporating receptor-factor interactions as

previously described) with restricted models (using only neuroimaging predictors and network propagation). The models including receptor maps and receptor-imaging interactions explained, on average, more than twice as much of the variance in longitudinal neuroimaging changes (Supplementary Table S7; $P<0.001$ with a two-sample t-test). To account for the greater explanatory power of a larger model with more parameters, we quantified the improvement in individual neuroimaging modeling due to the receptor terms, we conducted F-tests between the full re-MCM formulation (Fig. 2a) and the restricted model (Fig. 2b). As hypothesized, we observed that the inclusion of receptor maps and multi-scale (receptor-imaging) interaction terms significantly improved ($P<0.05$) the model accuracy for 86.8%-99.0% of the subjects (Fig. 2c) while accounting for the additional degrees of freedom in the model with receptors. While the inclusion of receptors and receptor-imaging interactions improved model performance for all subjects and modalities, this improvement was not always significant, most notably in 13.2% of gray matter atrophy models (Fig. 2c). We attribute this to the use of a shared, group-averaged set of neurotransmitter receptors templates (further tested below).

Having established that receptor maps and receptor-neuroimaging interactions do significantly improve personalized neuroimaging models, we then performed a permutation analysis on the receptor maps to test the informativeness compared model performance using averaged receptor templates to a set of null receptor maps. For each subject, the model fitting procedure was repeated using 1000 random permutations of the spatial receptor maps. Receptor densities were shuffled across regions of interest, independently for each receptor. We then compared the distribution of model fit (R^2) using these randomly permuted data with the R^2 obtained for the models using the true receptor templates. We observed that the significance of the improvement in model fitting over randomized receptor maps varied by imaging modality, for example, being lower for metabolism than for neural activity (Fig. 2d). Nevertheless, the true receptor templates perform significantly better in approximately 80%-98% of all subjects, depending on the modality. The gain in model performance by imaging modality is presented in Supplementary Table S8, and generally fell between $15.6\% \pm 13.3\%$ ($p<0.0417$) for glucose metabolism to $22.3\% \pm 15.0\%$ ($p<0.003$) for neural activity. Notably, the modalities for which true receptor data was the least informative (metabolism and gray matter atrophy), were also the ones for which augmenting the model with receptor data provided the least significant improvements across all subjects. Furthermore, we compared the proportion of subjects with significant improvements over null maps across diagnoses, shown in Supplementary Fig. S7. On average across modalities, 96.2% of healthy subjects' models were significantly improved, wheras this was progressively lower for MCI subjects (89.4% for early MCI and 89.8% for late MCI) and AD patients (78.3%).

We hypothesize that accentuated aging processes and neurodegeneration may alter receptor densities or interaction mechanisms in each individual, requiring the biological parameters in our personalized models to compensate. Identifying these specific alterations is the subject of the remaining subsections.

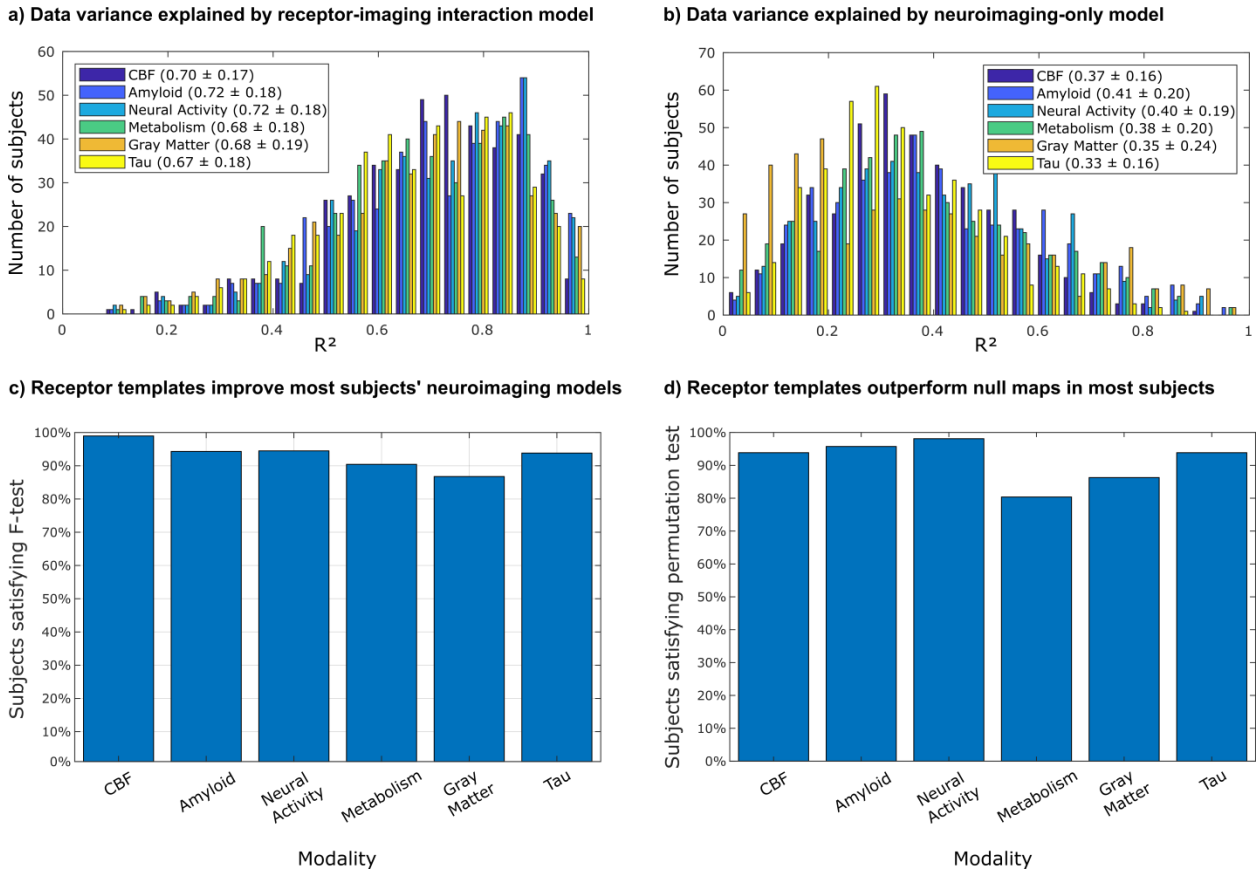

Figure 2: **Receptor density templates and multi-scale receptor-neuroimaging interactions significantly improve individual longitudinal neuroimaging models.** The improvement in neuroimaging modeling was evaluated in terms of i) including direct receptor terms and receptor-neuroimaging interactions in the model, and ii) using true receptor density maps compared to randomized, spatially permuted maps. The histograms in **(a)** and **(b)** show the distribution of the coefficient of determination (R^2) of N=423 individual models of neuroimaging changes including **(a)** and excluding **(b)** receptor predictors. Subject-specific linear models fit neuroimaging changes reasonably well, with a significant improvement by including receptor terms. This is confirmed by the F-test between subject models with and without receptor densities and receptor-imaging interactions (113 and 8 parameters, respectively). The proportion of subjects for whom the F-statistic is above the critical threshold is shown in **(c)**. This critical threshold corresponds to a statistically significant ($P<0.05$) improvement due to the receptor terms in the re-MCM model, accounting for the increase in adjustable model parameters. Furthermore, to validate the benefit of the receptor templates over randomized null maps, re-MCM models were fit with 1000 spatially-shuffled receptor maps for each subject. The p-value of the model fit (R^2) using true receptor templates compared to the distribution of R^2 of models using randomized templates was calculated for each subject. The proportion of subjects for whom the true receptor maps resulted in a statistically significant improvement in model fit ($P<0.05$) is shown in **(d)**. The results of these two analyses in **(c)** and **(d)** validate the use of averaged receptor templates in personalized neuroimaging models.

Characterizing receptor-imaging interaction variability in healthy aging and AD

We aimed to characterize the variability in receptor-mediated brain reorganization in the studied healthy aging (N=112) and AD subpopulations (N=25). In the healthy population, we performed a principal component analysis (PCA) on all re-MCM biological parameters (678 in total) across the 6 neuroimaging modalities, finding that the first principal component (PC1) is able to explain 97.3% of the group's variance. The most variable parameters contributing to PC1 belonged to CBF and gray matter models (Fig. 3a). That is, if current CBF in a region becomes less important (relative to other re-MCM predictors) to predicting its future change, gray matter density also becomes less important to predicting future atrophy, whereas the current level of amyloid becomes more important to predicting future accumulation. These results suggest that, in the absence of an influential disease process (e.g. neurodegeneration), inter-individual differences in the long-term brain reorganization are mechanistically driven by receptor-mediated processes affecting CBF and gray matter density. Most prominently, these include the CBF effects due to interactions between the dopaminergic D_1 receptor and amyloid distribution (2.9%), the adrenergic α_1 receptor and gray matter density (2.7%), the $GABA_A$ benzodiazepine site and neural activity ($GABA_A$/BZ; 2.0%), and the $GABA_A$ receptor and gray matter density (1.8%). Additionally, the interaction between the glutamatergic AMPA receptor and amyloid distribution as a predictor of gray matter atrophy (2.3%) are also notably variable.

In the AD group (N=25), with the presence of a neurodegenerative condition, the first PC of the re-MCM biological parameters only explained 26.2% of the population variability (with subsequent PCs explaining less than 10% each). Along this main axis of variability, inter-individual differences are primarily due the effects of neural activity as a direct or receptor-mediated predictor of tau accumulation (Fig. 3b; 7.9% of PC1 via the direct term, 7.3% via adrenergic $\alpha_1$receptors, 5.7% via serotonergic $5HT_{1A}$ receptors, 4.0% via dopaminergic D_1 receptors, and 3.7% via cholinergic $\alpha_4\beta_2$ receptors). The next subsection covers a deeper analysis of the AD group.

Interestingly, in the healthy subpopulation, when the individually small contributions of all receptor-terms for each target neuroimaging modality were summed (Fig 3c), we observed that the receptor mechanisms that affect CBF changes, gray matter atrophy and amyloid accumulation were the most variable, with GABAergic and serotonergic mechanisms dominating. For example, combined variability due to GABAergic (9.7% of PC1), serotonergic (8.7% of PC1) and adrenergic (primarily α_1 receptors; 7.3% of PC1) interactions predicting CBF changes accounted for approximately a quarter of variability across all 6 neuroimaging modalities and 678 total parameters (25.7% of PC1). As seen in Fig 3b, the main sources of biological parameter variability in AD (Fig 3d) involved neural activity predictors of tau accumulation. Predictors of tau accumulation involving adrenergic (9.9% of PC1), serotonergic (9.6%), cholinergic (6.6%) and dopaminergic (4.7%) interactions were the most variable.

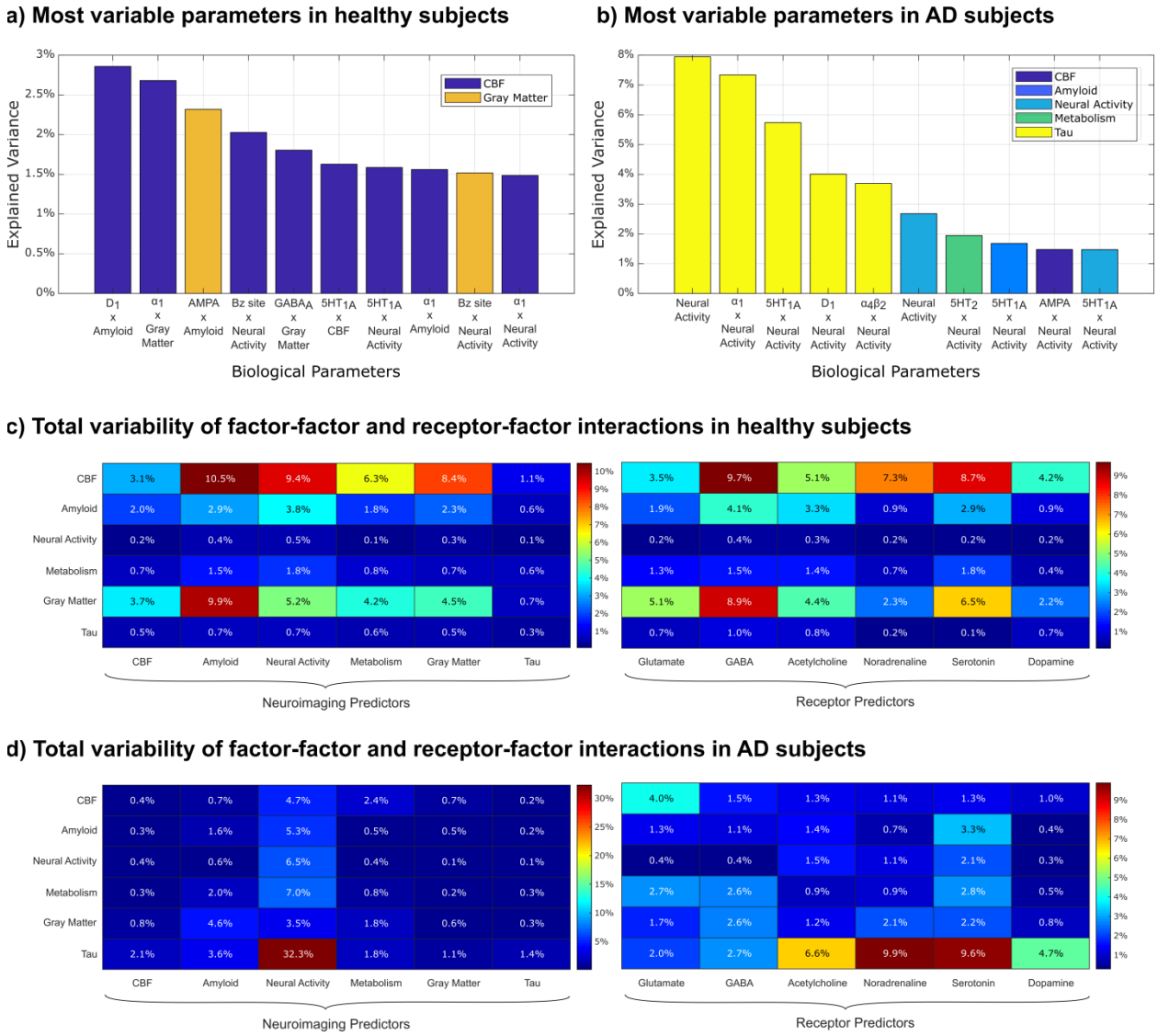

Figure 3: Variability of biological parameters across healthy and AD subjects. a-b) PCA-based sources of variability in the 678 re-MCM parameters across healthy subjects (N=112) and AD patients (N=25), respectively. The first principal component (PC1) captured 97.3% of the variance across parameters in healthy subjects, and 26.2% in AD patients. The top 10 biological parameters and their contributions to PC1 are plotted (with their target neuroimaging models in the legend), highlighting the receptor-imaging interactions that characterize the main axis of variability in each clinical subgroup. In healthy subjects, a multi-factorial combination of receptor-imaging interactions affecting atrophy and CBF changes were the most variable parameters along PC1. Notably, for AD patients, the top parameters were direct or receptor-mediated effects of neural activity on various (but especially tau) imaging models. **c-d)** To evaluate the relative importance of receptor- and factor-factor interactions, we then aggregated the importance of all direct or interaction terms involving a given predictor class (factor or receptor type) along PC1, for healthy subjects **(c)** and **(d)** for AD patients, respectively. Note that the percentage variation across all parameters is shown. As such, there is an overlap in terms

between the two heat maps (receptor-factor interaction terms contribute to both), and they should be interpreted separately.

Receptor-imaging alterations underlying cognitive deterioration in AD

To determine the receptor-neuroimaging alterations underlying multiple cognitive variations in AD, we performed a multivariate cross-correlation analysis between the rate of changes of the selected cognitive descriptors and the biological parameters across all AD subjects (*Materials and Methods: Biological parameters and relationship with cognition*). Notably, we found that just the first component of the identified biological parameters can explain up to 39.7% ($P<0.004$, FWE-corrected) of the inter-individual variability in AD cognitive deterioration (Figs. 4a). Furthermore, we identified the specific cognitive domains that are correlated with receptor-neuroimaging alterations (Fig. 4c), with executive dysfunction being the most salient cognitive feature with respect to receptor-neuroimaging parameters. Finally, Fig. 4d presents a detailed pathway of 95 receptor-imaging interactions significantly associated with cognitive decline based on feature bootstrapping, and their associated neuroimaging modalities mediating AD-related symptom severity. These results show that a multi-factorial set of molecular alterations are relevant to cognitive decline in AD. Cumulative effects of different neuroimaging interactions and receptor subtypes from the same family are summarized in Fig. 5, quantified by the total cognitive variance explained by all parameters of the relevant category via the significant SVD component.

Gray matter density (2.1%) and CBF (1.5%) changes as predictors of neural activity dysfunction, and CBF (1.3%) and glucose metabolism (1.0%) as predictors of tau distribution were the most cognitively-significant pathways between imaging modalities, although tau as a predictor of amyloid distribution (0.7%), neural activity dysfunction (0.7%) and glucose metabolism (1.2%) was also significant. Overall, as predictors, biological parameters involving CBF, tau and gray matter density were the most significant in relation to the cognitive severity of AD. The neuroimaging models of neural activity dysfunction and tau accumulation were the major sources of cognitively-significant biological parameters.

In terms of receptor systems, glutamatergic, GABAergic and cholinergic alterations were significant to cognitive decline, as summarized in Supplementary Table S6. Alterations to glutamatergic predictors of resting state functional activity (2.5%), GABAergic predictors of amyloid deposition (1.4%), and cholinergic predictors of tau distribution (1.4%) were the dominant receptor effects.

Furthermore, while the second component was borderline non-significant ($p<0.051$), it explained 23.4% of the variance between model parameters and cognitive decline ($r=0.89$, $p<10^{-8}$; Supplementary Fig. S10). In this axis, receptor-imaging parameters predicting neural activity were less prominent, with CBF and metabolism model parameters contributing more. Cognitively, this second component corresponded to non-executive function domains, primarily memory, language and visuospatial function.

As a control case, we performed an equivalent cross-correlation analysis in the healthy population, notably finding the first principal component relating re-MCM parameter with rates of cognitive decline in health to be non-significant (Supplementary Fig. S3), although the second

principal component explaining a small amount of cognitive variance was significant (15.5% variance explained, $p<0.02$; Supplementary Fig. S4). Furthermore, we found no significant component in amyloid-negative healthy subjects ($p>0.2$ for all components). We attribute this effect to the lack of consistent cognitive decline in the analyzed healthy population, in contrast to the large variability observed for AD.

To test the sensitivity of our findings to genetic covariates, we repeated our analyses both with and without APOE ε4 allele status and a polygenic hazard score (PHS) 49 as covariates in the SVD analysis, in addition to age, gender and education in both cases. To overcome the low number of AD subjects, we expanded our criteria to include MCI and AD subjects (N=177 for APOE status, N=161 for PHS). Importantly, we confirmed that the previously identified AD-related significant latent variables and parameters are robust to the inclusion of APOE status and PHS (Supplementary Fig. S5 and S6). Finally, to further restrict our analysis to subjects on the amyloid-mediated AD spectrum, we repeated the SVD analysis in amyloid positive subjects with MCI and AD (N=52). As was the case in the initial AD group, we found one significant principal component (44.3% variance explained, $p<0.003$) with a high correlation between model parameters and cognitive decline (mainly executive function; $r=0.76, p<0.001$). The main receptor-imaging interactions along this axis were analogous to those in the AD group, namely cholinergic predictors of tau accumulation, although parameters of the neural activity model were less prominent in favour of predictors of metabolism (particularly for adrenergic and cholinergic systems; see Supplementary Fig. S9).

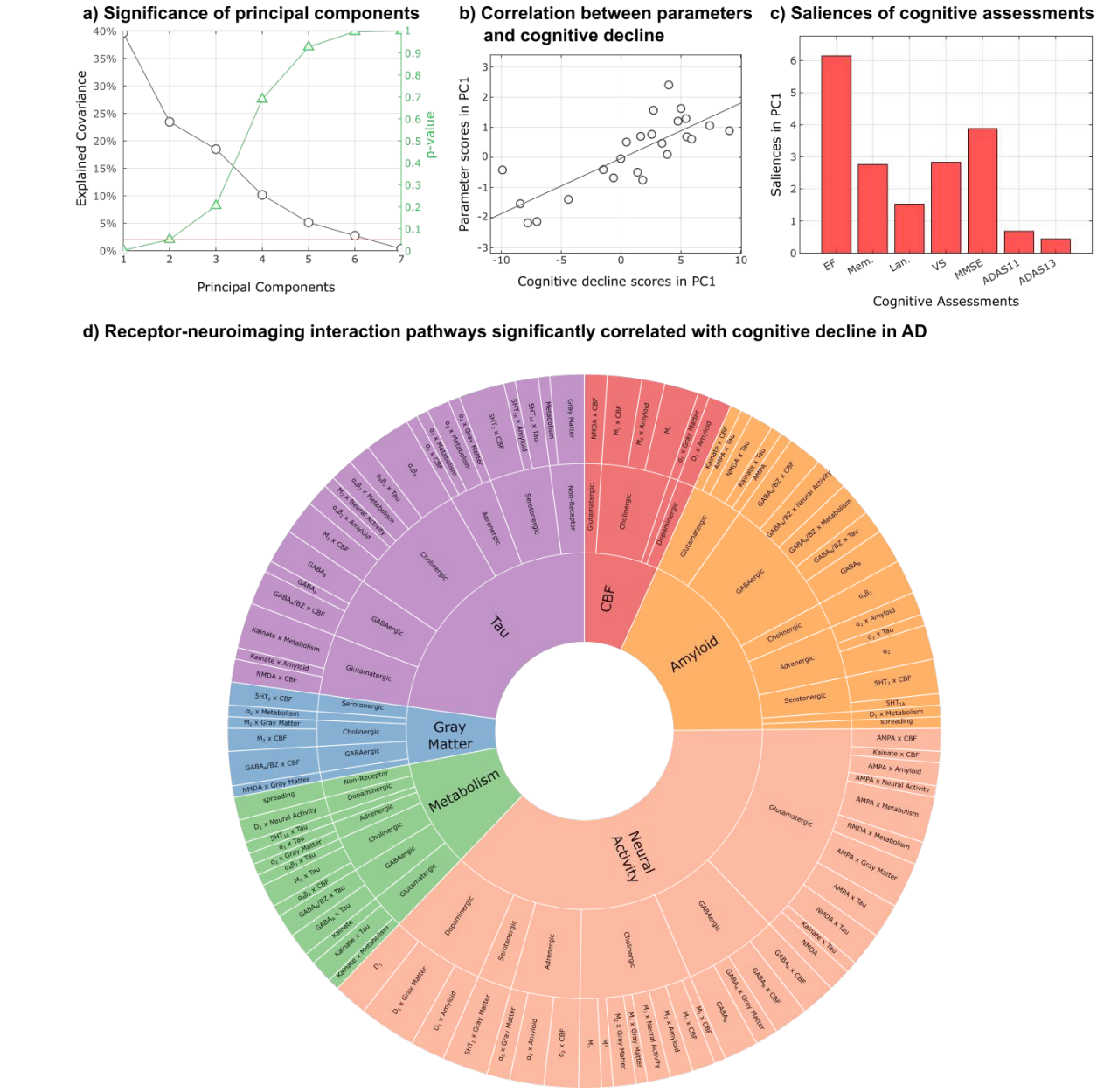

Figure 4: **Significant neurotransmitter receptor-imaging interactions underlying AD clinical severity. a)** The latent cross-correlation components are ranked by the fraction of cognitive decline variance explained by re-MCM biological parameters (along with the reported p-values based on the permutation analysis; see *Biological parameters and relationship with cognition*). In this case, only a single latent component was significant (39.7% variance explained, p<0.004, FWE-corrected). **b)** A notable correlation (r=0.80; $P<10^{-8}$) between the projections of statistically stable re-MCM parameters and rates of cognitive decline in the principal component space was observed, with the removal of an outlier subject more than 3 median absolute deviations from the median. **c)** Saliences of cognitive decline to this first latent component, providing a relative ranking of cognitive domains. These saliences are proportional to the contribution of each term relative to every other term, for example showing that executive dysfunction is most correlated with alterations to receptor-imaging interactions in AD. **d)**

Receptor-imaging pathways that are significantly correlated with cognitive decline, arranged by neuroimaging model and receptor type (Supplementary Table S5). The angle of each sector is proportional to the contribution of the corresponding parameter to explaining the variance in the rates of cognitive decline. The inner sectors represent the 6 neuroimaging modalities that together comprise each personalized re-MCM model. Within each modality, the intermediate sectors represent the neurotransmitter system involved, while the outer sector consists of the specific two-way receptor-neuroimaging interactions or direct predictor terms in the model. Notably, while receptors appear only as predictors in the outer sector, neuroimaging modalities appear both as predictors and as model outputs in the inner sectors. Thus, the relative importance of each neuroimaging modality to explaining cognitive differences is not fully represented by the angle of each inner sector.

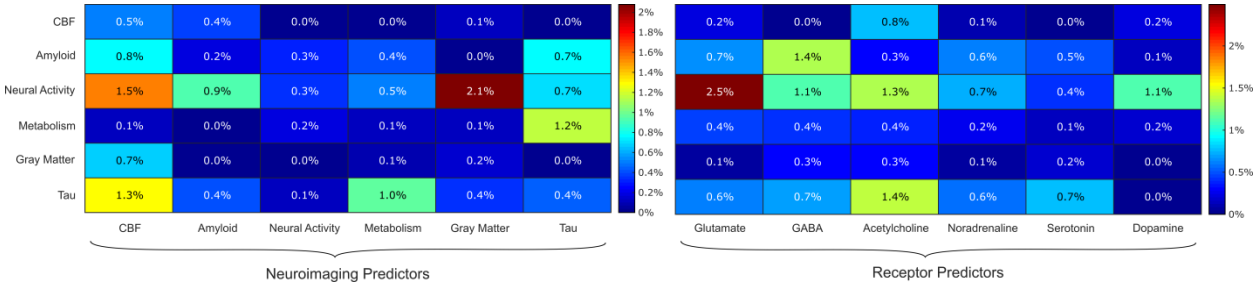

Figure 5: **Contributions of mechanistic pathways to the severity of cognitive decline in AD.** To better visualize the importance of neuroimaging factors and neurotransmitter receptor systems, heatmaps of the cumulative cognitive variance explained by each predictor category in each neuroimaging model are shown. These variances are the percentages of total cognitive variance that are explained by significant biological parameters of each category via the first significant SVD component. As such, the rows of the heatmap on the left replicate the inner sector of Fig. 4d, while the columns show the importance of each imaging modality or receptor family as predictors, with CBF and tau predictors explaining the most variance in cognitive decline.

Clinically-similar subjects have different underlying receptor alterations

Finally, for each participant and receptor family, we defined a summary metric quantifying how much receptor-based mechanisms differ from clinically healthy subjects (see *Statistical analysis: Inter-subject mechanistic variability*). For example, a given subject's glutamatergic Mahalanobis distance is a combined measure of the "unhealthiness" of receptor-based interactions and spatial distributions involving NMDA, AMPA and kainate, while accounting for the variation of these mechanisms in healthy subjects.

Although a simplified summary metric, the receptor Mahalanobis distances explained a large proportion of cognitive variance in the AD population, with 71.4% for executive function ($p<0.0004$), 43.3% for memory ($p<0.08$), 18.7% for language ($p<0.66$), 40.1% for visuospatial function ($p<0.10$), 43.8% for MMSE ($p<0.08$) and 33.8% for ADAS11 ($p<0.22$). Figure 6a shows the effects of each receptor family on cognitive domains, as well as the percentage

improvement in explaining cognitive variance due to each receptor family. We note the large negative effects of GABAergic alterations on executive function and the MMSE, and dopaminergic alterations on memory. Interestingly, cholinergic alterations showed a moderate positive effect and explanatory importance towards executive function.

In Figure 6b-c, we illustrate how two AD patients with similar cognitive symptoms present distinct receptor alteration fingerprints, with primarily glutamatergic and cholinergic mechanisms respectively. Importantly, this result suggests that even subjects with identical clinical diagnoses present distinctive underlying spatiotemporal molecular alterations, and supports the use of whole-brain generative models to uncover patient-specific receptor and potential disease mechanisms to target clinically.

a) Improvement in prediction of cognitive decline in AD due to each receptor family

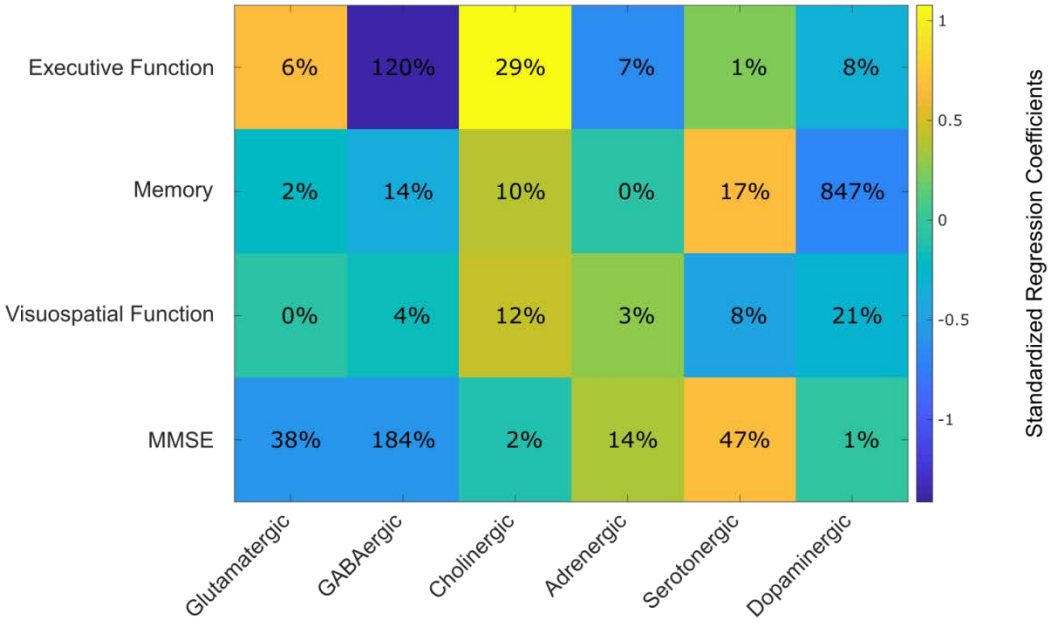

b) Similar cognitive symptoms

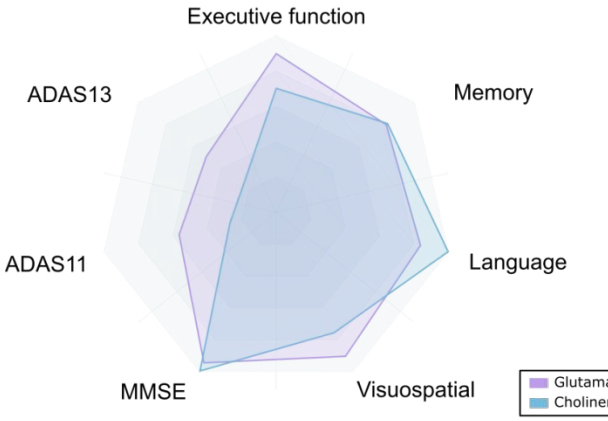

c) Distinct receptor alterations

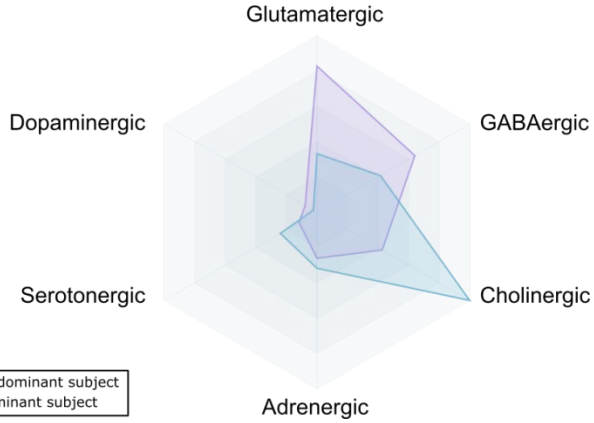

Figure 6: **Receptor alterations underlying inter-individual disease heterogeneity. a)** In AD patients (N=25), we quantified the relative effect sizes of standardized Mahalanobis distances of receptor mechanisms on different cognitive domains. We also standardized the regression coefficients within each cognitive domain before visualizing to facilitate comparison across cognitive domains, and the percentage improvement in model fit (R^2) due to each receptor system is also shown. For example, the explanation of inter-subject variability in executive function decline by glutamatergic, cholinergic, adrenergic, serotonergic and dopaminergic Mahalanobis distances is improved by 120% (i.e. more than doubled) by the inclusion of GABAergic Mahalanobis distance as well. **b-c)** We show two AD subjects, with similar symptoms across a variety of cognitive domains. For these subjects, we calculated the Mahalanobis distance to the distribution of all healthy subjects (N=112), along mechanisms involving each receptor family. The subjects show distinct receptor alterations based on their longitudinal neuroimaging changes, despite their shared designation as AD patients and similar cognitive profiles.

Discussion

In this work, we have presented a personalized, whole-brain and generative multi-modal neuroimaging model incorporating receptor-neuroimaging interactions using *in-vivo* data. Subsequent analyses on the resulting models have allowed, for the first time, the identification of i) variability in receptor-neuroimaging interactions in healthy subjects and AD patients, and ii) specific pathways of receptor-neuroimaging interactions that are important to cognitive decline in AD patients. This exploratory analysis provides a bridge between molecular-level mechanisms and observable macroscopic neuroimaging biomarkers of healthy aging and AD, revealing which neurotransmitter receptor systems mediate dysfunctional interactions between neurobiological processes such as cerebral blood flow, amyloid and tau deposition, gray matter atrophy, neural activity and metabolism.

Due to the difficulty of comprehensive, personalized *in vivo* receptor imaging for a large cohort, receptor maps were not specific to each subject, but instead the averaged templates of 4 post-mortem brain samples. Post-mortem *in vitro* autoradiography allowed the imaging of a large number of receptor types, even those without *in vivo* radioligands. Firstly, our work demonstrates that i) multi-scale interaction terms involving the spatial distributions of neurotransmitter receptors are highly informative to models of neuroimaging progression, and ii) even group-averaged receptor map templates can significantly improve the personalized model fit in nearly all subjects when combined with personalized neuroimaging predictors. Specifically, incorporating receptor maps and multi-scale receptor-imaging interactions to personalized models with multi-modal neuroimaging predictors improves the average data variance explained from approximately 40% to 70% (Fig. 2a,b). This improvement is statistically significant (F-test with $P<0.05$) in almost all subjects (Fig. 2c), even after accounting for the additional predictive power of the larger, multi-scale models. Including only receptor maps without receptor-imaging interactions also resulted in a more modest yet significant improvement in the vast majority of subjects across all imaging modalities (Supplementary Fig. S2). This is a particularly strong result, validating the use of a group-averaged receptor template, given the large improvement and the stringent criterion accounting for additional model parameters.

Additionally, models using the true receptor templates perform significantly better ($P<0.05$ of R^2) than models using randomly permuted, null receptor maps in almost all subjects (Fig 2d; 80.4%-98.1%, depending on the modality), although this improvement was less evident with disease progression (Supplementary Fig. S7). These results, along with the consistency of regional receptor densities across the 4 (aged but healthy) brains used to produce the templates compared to inter-region variability [35], support the applicability of receptor templates to a wider population. Receptor mapping studies across more diverse clinical groups of patients would help validate or augment our modeling approach. Nevertheless, given the difficulty of acquiring a wide variety of *in-vivo* molecular data, due to a limited number of appropriate radioligands, and the high cost of longitudinal molecular imaging, these results on model accuracy are a promising validation for the combination of other molecular templates (such as gene expression atlases) with personalized neuroimaging predictors. These "pseudo-personalized" molecular-imaging predictors can then be incorportated into neuroimaging models and used to infer mechanistic alterations in a group of subjects. If these personalized models are sufficiently accurate, as in this work, the weights of their biological parameters then serve as proxies for individual-specific alterations to receptor-mediated mechanisms.

While interpreting these parameters, it is important to distinguish between the types of biological mechanisms they represent, which include (for each neuroimaging model) i) direct neuroimaging effects, ii) direct receptor density effects, iii) receptor-imaging interactions, iv) network propagation and v) offset terms representing an intrinsic rate of change for the neuroimaging modality. We hypothesize that ageing and neurodegeneration alter the spatial distributions of and functional interactions involving neurotransmitter receptors, which would lead to subject-specific model parameters to compensate in the absence of inter-subject variability in receptor data. Thus, model parameters are a proxy for alterations to spatial maps of receptors or their interactions with neurobiological processes (represented by direct model receptor density terms and receptor-imaging interaction terms in the model, respectively). In our parameter analyses in *Receptor-imaging alterations underlying cognitive deterioration in AD*, direct receptor density terms represent alterations to the spatial distribution of a particular receptor. Each interaction biological parameter value can be interpreted as the effect of the corresponding receptor or imaging factor on the brain reorganization process, as measured by neuroimaging changes, given "normal" (i.e. spatial mean) values of all related predictors involving the same receptor or imaging term, respectively. For example, we consider the case where the interaction term between a glutamatergic receptor and amyloid in the CBF model is significantly related to cognitive decline. This implies that, under normal levels of amyloid and the glutamatergic receptor individually, a functional alteration in this mechanism (quantified by the re-MCM parameter weight) is correlated with faster cognitive deterioration.

Biological parameters were evaluated for principal axes of variability in Fig. 3 and the cognitively-relevant variability in Fig. 4. The former method was used to identify linear combinations of biological parameters that accounted for inter-individual differences in receptor and/or neuroimaging interaction strengths in healthy and AD subjects. On the other hand, the goal of the latter analysis was to identify biological parameters that were robustly correlated with multivariate measures of cognitive decline in AD. The purpose of these analyses was not to compare effects sizes between predictors, but rather to explore inter-subject differences in receptor-imaging interactions in relation to cognitive decline. For example, if regional amyloid accumulation strongly predicts changes in functional activity, but this biological parameter is

consistent across subjects with different clinical and cognitive states, it would not be significant to our analysis. Rather than using clinical diagnosis, which is subject to large variability due to patient presentation and clinician bias, we used a combination of cognitive test scores. Ultimately, cognitive performance is the phenotype of interest in neurodegeneration. Our SVD analysis allows us to identify parameters associated with cognitive scores, rather than simply those with a large variability between individuals due to other causes.

Sources of variability in healthy and AD subjects (Fig. 3) reflect alterations to mechanisms of receptor-imaging interaction that predict the same or another imaging modality. Here, we observed that a single PCA component explains 97.3% of the inter-individual variability in healthy subjects. Along this axis, a multi-faceted combination of receptor-imaging interaction predictors of CBF alterations (e.g. the interaction between dopaminergic D_1 receptors and amyloid) and gray matter atrophy (e.g. the interaction between glutamatergic AMPA receptors and amyloid) account for the majority of variability (Fig. 3a,c). Interestingly, there is relatively low variability in the biological parameters of receptor influence on neural activity, glucose metabolism and tau distribution in healthy individuals (Fig. 3c). In healthy subjects, the receptor-imaging mechanisms affecting these factors are comparatively consistent, whereas the mechanisms behind atrophy, CBF regulation and amyloid accumulation display more inter-subject heterogeneity.

In contrast, the first principal component of AD subjects' biological parameters explained only 26.2% of the total variance, but this was dominated by neural activity as a (receptor-modulated) predictor of tau accumulation (as well as other neuroimaging modalities; Fig. 3b,d). Receptor mechanism variability was largely explained by adrenergic and serotonergic predictors, for example the interactions of α_1 and $5HT_{1A}$ receptors with neural activity to predict tau accumulation. As tau is primarily present in axonal microtubules, the exacerbation of tau pathology has been linked to enhanced neural activity [50]. Conversely, tau is also believed to suppress and silence neural activity [22]. Thus, the principal component of variability in AD subjects may represent variability in an activity-dependent tau accumulation via adrenergic α_1, serotonergic $5HT_{1A,}$ dopaminergic D_1, and cholinergic $\alpha_4\beta_2$ receptors. This would be consistent with the observed mediation of tau hyperphosphorylation by adrenergic and serotonergic receptors in animal models [51] 52.

From the inner sectors of Fig. 4d, inter-individual differences in cognitive decline are most correlated with biological parameters of the neural activity, tau and amyloid models, and least correlated with biological parameters of the CBF, gray matter density and glucose metabolism models. In other words, differences in receptor-imaging interactions affecting CBF changes are less relevant to cognitive symptom severity in AD than those affecting resting state functional activity. While neural activity is not a cognitively-important predictor of other neuroimaging modalities, many predictors of neural activity dysfunction are correlated with cognitive severity in AD (Fig. 5). Conversely, predictors of CBF do not vary significantly with cognition, whereas CBF itself is an important predictor of many other neuroimaging modalities. This may imply a causal ordering, with CBF alterations preceding dysfunctional activity.

The glutamatergic system is implicated in cognitive decline via its role as the major excitatory mediator of neural activity [53 54 55]. In AD, the glutamatergic system is involved in excitotoxicity due to calcium ion influx via NMDA receptors 53, resulting in synaptic loss and neuronal cell death [54]. Tau and amyloid are involved via an overactivation of NMDA receptors [56]. The

synaptic activation of NMDA receptors is linked to specific neurophysiological conditions, particularly activity-dependent synaptic plasticity, as well as behavioural symptoms of multiple brain disorders including AD [57]. In addition, AMPA receptors are involved in synaptic scaling, and consequently learning and memory. Reductions in AMPA receptor levels have been observed in mouse models of AD [58], as well as in the entorhinal cortices [59] of AD patients, with a differential preservation of certain subunits in the hippocampus [60], and AMPA receptor endocytosis has been linked to the phosphorylated tau signaling cascade [61]. Thus, the established AD-related alterations and cognitive roles of the glutamatergic NMDA and AMPA receptors would be consistent with their significant modulation of resting state functional activity in relation to cognitive decline in AD via interactions with CBF, glucose metabolism and tau.

From the columns of Fig. 5, CBF changes are the largest neuroimaging driver of cognitively-relevant dysfunction in other modalities, consistent with its precedence among AD imaging biomarkers [10]. Closely coupled to neural activity, CBF is mediated by several neuronal factors, including vasodilatory neurotransmitters, and vascular dysregulation is implicated in the pathogenesis of AD [62]. CBF interactions with a multitude of receptors were correlated to cognitive severity via amyloid, neural activity, gray matter density and tau models. This is consistent with the amyloid-dependent relationship of CBF to memory performance [63], and the link to tau pathology via gene expression alterations in AD [64].

Furthermore, inter-individual differences in the effects of tau on other imaging modalities are also major contributors to AD-associated cognitive decline, as seen in Fig. 5. These include glutamatergic interactions affecting neural activity and amyloid accumulation, and a multifactorial set of receptor interactions affecting metabolism. Cognitive decline in AD is accompanied by changes in the role of regional tau concentration as a predictor of amyloid distribution, suggesting synergistic or mediation effects such as the tau axis hypothesis 65. Tau is believed to mediate amyloid toxicity [65], which may explain the significant role of tau as a predictor of amyloid accumulation (Fig. 5). Multimodal PET imaging has shown a region-dependent relationship between tau burden and hypometabolism in AD [66]. Futhermore, alterations to glucose metabolism in mice brains were found to lead to abnormal tau hyperphosphorylation [67]. Along with the established neural activity dysfunction due to tau accumulation [68], these mechanisms are consistent with the cognitively-significant role of tau as a predictor of other neuroimaging modalities.

Along with NMDA, acetylcholine is the neurotransmitter system most associated with Alzheimer's disease and its clinical treatment [69]. Based on the cholinergic hypothesis, dysfunction in acetylcholine-producing basal forebrain regions would eventually lead to synaptic deafferentiation in the cortical regions to which they project [70], with cognitive implications [71]. This is consistent with the significant role of cholinergic predictors of tau distribution, which appear to be more correlated with cognitive severity of AD than amyloid distribution (Fig. 5).

Although GABAergic receptors were not initially linked to AD, recent evidence has uncovered disease-related alterations, contributions to pathogenesis, and a potential therapeutic role in AD [72]. The disruption of the excitatory/inhibitory balance maintained by GABAergic signaling has been implicated in the cognitive symptoms of AD, such as an increase in epileptic seizures [73]. Electrophysiological activity has found a functional remodeling of GABAergic neurons in AD, showing reduced currents and a faster rate of desensitization [74]. The presence of amyloid was also found to affect the expression of the α_6 subunit of the $GABA_A$ receptor [72]. Furthermore, a

role for tau has been proposed in the regulation of GABAergic function and synaptic plasticity to maintain normal cognition [73]. Additionally, it has recently been found that the administration of benzodiazepine in mouse brains leads to tau hyperphosphorylation [75]. Such drugs potentiate GABAergic neurotransmission by binding to the benzodiazepine binding site of $GABA_A$ receptors. As such, this may indicate a mechanistic pathway for the induction of tau pathology involving GABAergic receptors, based on the tau and gray matter sectors of Fig. 4d. From Fig. 4d, the $GABA_A$-associated benzodiazepine site is particularly involved in cognitively-significant interactions affecting amyloid accumulation. $GABA_A$ and $GABA_B$ receptors play a notable cognitive role by affecting neural activity dysfunction, and all three GABAergic targets included in this work are involved via tau accumulation.

Finally, we introduced a summary metric of alterations to receptor-mediated interactions with reference to their normal variation in healthy ageing. Particularly, we found that GABAergic alterations had the largest effect on cognitive impairment in AD patients, significantly affecting executive function and the MMSE (Fig. 6a). Furthermore, we showed that subjects with identical clinical diagnosis and similar cognitive symptoms can have distinct underlying dynamics and receptor alteration fingerprints (Fig. 6b-c). These results highlight the clinical utility of our dynamical modeling approach. By fusing *in vitro* receptor templates with longitudinal neuroimaging data and modeling the underlying dynamics of receptor-mediated neurobiological interactions, we are able to infer subject-specific mechanistic alterations despite the lack of subject-specific receptor data. As a demonstrative example, we summarized subject-specific alterations at the scale of receptor families. However, in a clinical context, subject-specific alterations at the broad scale of receptor families, the finer scale of specific receptors, or even specific receptor-neurobiological interactions (e.g. NMDA × CBF interactions) can be used to design personalized, precision treatments, which will be a topic of future work.

The whole-brain re-MCM models used cytoarchitectonically-identified cortical regions of interest, neglecting sub-cortical structures for which no receptor distribution data was available. Many neurotransmitter alterations relevant to neurodegeneration occur in these regions, notably dopamine deficiencies in the basal ganglia in Parkinson's disease and early cholinergic neuronal death in AD. As such, including sub-cortical regions may better characterize important molecular pathways. Nevertheless, some effects of these phenomena are captured via projections to cortical neurons that are covered by our regions of interest. Additionally, future work will aim to integrate CSF into the model.

In this work, we used fractional amplitude of low-frequency fluctuation (fALFF) [31] as the regional measure of functional integrity. Low frequency (0.01-0.08 Hz) oscillations in the blood oxygenation level-dependent (BOLD) signal reflect the intensity of spontaneous activity in the resting brain, primarily in the default mode network [31]. When the amplitude of low frequency fluctuations (ALFF) is normalized by the overall power spectrum of the BOLD signal to calculate fALFF, the effects of physiological noise are suppressed [31]. However, compared to ALFF, fALFF significantly amplifies the signal from some non-default mode network regions (namely temporal-parietal regions and the precentral gyrus) [31], reducing its desired specificity to resting state activity. Nevertheless, fALFF shows high temporal stability over the course of fMRI scans [76], long-term (i.e. about 6 month) test-retest reliability [77], and high sensitivity to AD progression [29] [30]. Alternative fMRI-based metrics include regional homogeneity (ReHo) [78] or graph theoretic metrics such as functional connectivity degree [79]. Comparing fALFF, ReHo, and graph-based metrics using simultaneous resting state fMRI/PET scans, Aiello et al. found

functional connectivity degree to be the least correlated to glucose uptake, while the difference in correlation to glucose uptake between fALFF and ReHo was not significant [28]. Furthermore, as an intentional consideration to maintain model interpretability, our modeling framework avoids graph theoretic fMRI metrics in order to separate local, intra-region effects from inter-region effects due to network propagation. Although graph theoretic features can have biophysical interpretation, such as weighted degree representing transneural propagation or regional participation coefficients reflecting metabolic demands, they integrate information from multiple regions, which causes a leakage of network information into the intra-regional component of our model. Thus, as fALFF is a local fMRI measure that has been found to be at least as informative as ReHo in reflecting metabolic activity and validated as a measure sensitive to AD progression by multiple studies [29 30], all the analyses and results presented in this study correspond to fALFF as the measure of resting state functional integrity. It is, however, important to note that all available fMRI metrics have limitations in reflecting actual neuronal activity or integrity. Here, our choice of metric is aligned with the "neurocentric" resting-state fMRI model [80], which assumes that the spontaneous fluctuations in BOLD signal reflect ongoing neuronal processes. Multiple limitations to this model have been pointed out, including the lack of clear neurophysiological interpretability [80], suggesting that interpretations of resting state fMRI-based findings (including ours) should be taken with caution.

In addition to intra-region effects, our model considered network propagation along the tractography-derived white matter structural connectome. However, functional, metabolic [81] and vascular connectivity define complementary biophysical networks that may also contribute to the propagation of neurodegenerative pathology. For simplicity and to focus on local, receptor-mediated interactions, we restricted our model to structural connectivity. The structural connectome is the physical substrate for the axonal propagation of pathology, and the scaffolding for the more abstract functional network. However, to estimate the effect of our choice of connectivity, we repeated our model fitting with functional connectivity, finding no significant change in model fit (*Multi-scale interactions involving neurotransmitter receptors are important to explaining multifactorial brain reorganization* and Supplementary Fig. S8). We attribute this to (i) the dominance of intra-regional effects in our model, with a relatively low contribution due to propagation effects and (ii) the shared information between anatomical and functional connectivity [48]. While this work has focused on local interactions between biological processes, dynamical interactions also occur at a network level. For example, structural connectivity [82] and the vascular network [83] are two of the factors that shape functional connectivity, and modeling the dynamic interactions between these networks may be a potential direction for future work.

The dynamical system modeling approach in this work relies on longitudinal and multi-modal neuroimaging data in order to fit personalized models. Consequently, our results would benefit from larger cohorts with more longitudinal samples of multi-modal data. Additionally, receptor map templates of patients at different stages of aging and disease progression would improve the characterization of salient alterations. While we have attempted to uncover causal molecular-macroscopic mechanisms, due to the lack of personalized, longitudinal receptor maps, some identified biological model parameters may in fact reflect a molecular alteration (i.e. a change in either spatial distribution or functional alteration of a receptor) in response to a change in a macroscopic biological variable. As such, the exploratory interpretation of our results in relation to cognitive decline in AD should account for both possible causal directions between a given biological parameter and its target modality. For example, α_1 receptors interacting with tau to

predict functional activity represents a 3-way interaction, which may in fact reflect a causal direction from functional activity to adrenergic alteration. Furthermore, we have assumed a direct relationship between each imaging modality and an underlying neurobiological process. For instance, CBF in our model was derived from ASL MRI, the temporal resolution of which is limited by the relaxation time of blood. However, recent work on venous blood flow using BOLD perfusion lag-mapping has shown significant age-related changes outside the temporal resolution of ASL MRI [84]. As new or improved imaging biomarkers are developed for AD, their future inclusion in the re-MCM framework would improve the coverage of potential disease-related mechanisms.

Nevertheless, these results offer interpretable results via molecular targets and mechanisms of action. We find that receptor distributions mediate interactions between macroscopic biological factors that significantly affect cognitive decline in AD. Specifically, inter-individual differences in cognitive deterioration correlate with the modulation of neural activity dysfunction primarily by glutamatergic receptors, amyloid accumulation by GABAergic receptors, and tau buildup by glutamatergic, GABAergic and cholinergic receptors. Traditionally, the accumulation of misfolded proteins, namely amyloid and tau, has been implicated in the pathogenesis of AD. However, our results suggest a multi-factorial, and heterogeneous set of mechanisms involved in disease. Furthermore, our personalized, data-driven approach allows us to account for inter-subject heterogeneity in biological pathology and clinical presentation.

A growing body of evidence supports the critical role of neurotransmitter receptors in AD symptoms severity and their subsequent potential as therapeutic targets [85 86]. Neurotransmitter-based drugs such as the acetylcholinesterase inhibitor donepezil and the NMDA antagonist memantine have long been proposed as potential treatments for AD patients. However, these drugs have shown limited efficacy and adverse side effects [20] 56. We propose that using personalized and multi-scale modeling can identify patient-specific alterations and therapeutic needs, by stratifying patients based on the biological parameter weights corresponding to the underlying, cognitively-significant mechanisms (Figs. 1c and 6). This information can then be used to design individually-tailored multi-factorial therapies to slow the process of cognitive decline in both diseased and normally-ageing individuals.

Funding

This research was undertaken thanks in part to funding from: the *Canada First Research Excellence Fund*, awarded to McGill University for the *Healthy Brains for Healthy Lives Initiative*, the Canada Research Chair tier-2, *Fonds de la recherche en santé du Québec* (FRQS) Junior 1 Scholaship and Weston Brain Institute (Rapid Response AD program 2018) awards to YIM, the *Brain Canada Foundation* and *Health Canada* support to the McConnell Brain Imaging Center at the Montreal Neurological Institute, and the *European Union's Horizon 2020 Framework Programme for Research and Innovation* under the Specific Grant Agreements 785907 (Human Brain Project SGA2) and 945539 (Human Brain Project SGA3) awarded to NPG and KZ. Multimodal imaging and clinical data collection and sharing for this project was funded by ADNI (National Institutes of Health Grant U01 AG024904) and DOD ADNI (Department of Defense award number W81XWH-12-2-0012). ADNI is funded by the National Institute on Aging, the National Institute of Biomedical Imaging and Bioengineering, and through generous contributions from the following: AbbVie, Alzheimer's Association;

Alzheimer's Drug Discovery Foundation; Araclon Biotech; BioClinica, Inc.; Biogen; Bristol-Myers Squibb Company; CereSpir, Inc.; Eisai Inc.; Elan Pharmaceuticals, Inc.; Eli Lilly and Company; EuroImmun; F. Hoffmann-La Roche Ltd and its affiliated company Genentech, Inc.; Fujirebio; GE Healthcare; IXICO Ltd.; Janssen Alzheimer Immunotherapy Research & Development, LLC.; Johnson & Johnson Pharmaceutical Research & Development LLC.; Lumosity; Lundbeck; Merck & Co., Inc.; Meso Scale Diagnostics, LLC.; NeuroRx Research; Neurotrack Technologies; Novartis Pharmaceuticals Corporation; Pfizer Inc.; Piramal Imaging; Servier; Takeda Pharmaceutical Company; and Transition Therapeutics. The Canadian Institutes of Health Research is providing funds to support ADNI clinical sites in Canada. Private sector contributions are facilitated by the Foundation for the National Institutes of Health (www.fnih.org). The grantee organization is the Northern California Institute for Research and Education, and the study is coordinated by the Alzheimer's Disease Cooperative Study at the University of California, San Diego. ADNI data are disseminated by the Laboratory for Neuro Imaging at the University of Southern California.

Competing Interests

The authors report no competing interests.

Supplementary material

Supplementary material is available at *Brain* online.

References

1. Francis PT, Ramírez MJ, Lai MK. Neurochemical basis for symptomatic treatment of alzheimer's disease. *Neuropharmacology*. 2010;59(4-5): 221–229.

2. Jack Jr CR, Knopman DS, Jagust WJ, et al. Hypothetical model of dynamic biomarkers of the alzheimer's pathological cascade. *The Lancet Neurology*. 2010;9(1):119–128.

3. Lam B, Masellis M, Freedman M, Stuss DT, Black SE. Clinical, imaging, and pathological heterogeneity of the alzheimer's disease syndrome. *Alzheimer's research & therapy*. 2013;5(1):1.

4. Iturria-Medina Y, Carbonell FM, Evans AC. Multimodal imaging-based therapeutic fingerprints for optimizing personalized interventions: Application to neurodegeneration. *NeuroImage*. 2018;179:40-50.

5. Kosik KS. Personalized medicine for effective alzheimer disease treatment. *JAMA Neurology*. 2015;72(5):497-498.

6. Schork NJ. Personalized medicine: Time for one-person trials. *Nature*. 2015;520(7549):609-611.

7. Prakash A, Kalra J, Mani V, Ramasamy K, Majeed ABA. Pharmacological approaches for alzheimer's disease: Neurotransmitter as drug targets. *Expert review of neurotherapeutics*. 2015;15(1):53-71.

8. Roy K. *Computational modeling of drugs against Alzheimer's disease*: Springer; 2018.

9. Jack Jr. CR, Knopman DS, Jagust WJ, et al. Tracking pathophysiological processes in Alzheimer's disease: an updated hypothetical model of dynamic biomarkers. *The Lancet Neurology*. 2013;12(2):207-216.

10. Iturria-Medina Y, Sotero RC, Toussaint PJ, Mateos-Pérez JM, Evans AC, Initiative tADN. Early role of vascular dysregulation on late-onset Alzheimer's disease based on multifactorial data-driven analysis. *Nature Communications*. 2016;7(1):1-14.

11. Iturria-Medina Y, M.Carbonell F, Sotero RC, Chouinard-Decorte F, C.Evans A. Multifactorial causal model of brain (dis)organization and therapeutic intervention: Application to Alzheimer's disease. *NeuroImage*. 2017;152:60-77.

12. Moses WW. Fundamental limits of spatial resolution in PET. *Nuclear Instruments and Methods in Physics Research Section A: Accelerators, Spectrometers, Detectors and Associated Equipment*. 2011;648:S236-S240.

13. Choi JK, Chen YI, Hamel E, Jenkins BG. Brain hemodynamic changes mediated by dopamine receptors: Role of the cerebral microvasculature in dopamine-mediated neurovascular coupling. *Neuroimage*. 2006;30(3):700-712.

14. Iadecola C. Neurovascular regulation in the normal brain and in Alzheimer's disease. *Nature Reviews Neuroscience*. 2004;5(5):347-360.

15. Mink JW, Blumenschine RJ, Adams DB. Ratio of central nervous system to body metabolism in vertebrates: Its constancy and functional basis. *American Journal of Physiology-Regulatory, Integrative and Comparative Physiology*. 1981;231(3):R203-R212.

16. Harris JJ, Jolivet R, Attwell D. Synaptic energy use and supply. *Neuron*. 2012;75(5):762-777.

17. McCann CM, Tapia JC, Kim H, Coggan JS, Lichtman JW. Rapid and modifiable neurotransmitter receptor dynamics at a neuronal synapse in vivo. *Nature neuroscience*. 2008;11(7):807.

18. Mora F, Segovia G, del Arco A. Aging, plasticity and environmental enrichment: structural changes and neurotransmitter dynamics in several areas of the brain. *Brain research reviews*. 2007;55(1):78-88.

19. Heiss WD, Herholz K. Brain receptor imaging. *Journal of Nuclear Medicine*.

2006;47(2):302-312.

20. Kandimalla R, Reddy PH. Therapeutics of neurotransmitters in alzheimer's disease. *Journal of Alzheimer's Disease*. 2017;57(4):1049-1069.

21. Bejanin A, Schonhaut DR, La Joie R, et al. Tau pathology and neurodegeneration contribute to cognitive impairment in Alzheimer's disease. *Brain*. 2017;140(12):3286-3300.

22. Busche MA, Wegmann S, Dujardin S, et al. Tau impairs neural circuits, dominating amyloid-β effects, in Alzheimer models in vivo. *Nature neuroscience*. 2019;22(1):57-64.

23. Sled JG, Zijdenbos AP, Evans AC. A nonparametric method for automatic correction of intensity nonuniformity in MRI data. *IEEE transactions on medical imaging*. 1998;17(1):87–97.

24. Evans AC, Kamber M, Collins D, MacDonald D. An MRI-based probabilistic atlas of neuroanatomy. *Magnetic resonance scanning and epilepsy*. 1994:263-274.

25. Ashburner J. A fast diffeomorphic image registration algorithm. *NeuroImage*. 2007;38(1):95-113.

26. Jagust WJ, Bandy D, Chen K, et al. The Alzheimer's Disease Neuroimaging Initiative positron emission tomography core. *Alzheimer's & Dementia*. 2010;6(3):221-229.

27. Yan C, Zang Y. DPARSF: A matlab toolbox for "pipeline" data analysis of resting-state fMRI. *Frontiers in systems neuroscience*. 2010;4:13.

28. Aiello M, Salvatore E, Cachia A, et al. Relationship between simultaneously acquired resting-state regional cerebral glucose metabolism and functional MRI: a PET/MR hybrid scanner study. *Neuroimage*. June 2015(113):111-121.

29. Yang L, Yan Y, Wang Y, et al. Gradual disturbances of the amplitude of low-frequency fluctuations (ALFF) and fractional ALFF in Alzheimer spectrum. *Frontiers in neuroscience*. 2018;12:975.

30. de Vos F, Koini M, Schouten TM, et al. A comprehensive analysis of resting state fMRI measures to classify individual patients with Alzheimer's disease. *Neuroimage*. February 2018;15(167):62-72.

31. Zou QH, Zhu CZ, Yang Y, et al. An improved approach to detection of amplitude of low-frequency fluctuation (ALFF) for resting-state fMRI: Fractional ALFF. *Journal of neuroscience methods*. 2008;172(1):137-141.

32. Palomero-Gallagher N, Zilles K. Cyto-and receptor architectonic mapping of the human brain. *Handbook of clinical neurology*. 2018;150:355-387.

33. Merker B. Silver staining of cell bodies by means of physical development. *Journal of neuroscience methods*. 1983;9(3):235-241.

34. Eickhoff SB, Paus T, Caspers S, et al. Assignment of functional activations to probabilistic cytoarchitectonic areas revisited. *NeuroImage*. 2007;36(3):511-521.

35. Zilles K, and Palomero-Gallagher N. Multiple transmitter receptors in regions and layers of the human cerebral cortex. *Frontiers in neuroanatomy*. 2017;11:78.

36. Brodmann K. *Vergleichende Lokalisationslehre der Grosshirnrinde in ihren Prinzipien dargestellt auf Grund des Zellenbaues*. Leipzig: Barth JA; 1909.

37. Jenkinson M, Beckmann CF, Behrens TE, Woolrich MW, Smith SM. FSL. 2012;62:782-90.

38. Yeh FC, Panesar S, Fernandes D, et al. Population-averaged atlas of the macroscale human structural connectome and its network topology. *NeuroImage*. 2018;178:57-68.

39. Yeh FC, Tseng WYI. NTU-90: A high angular resolution brain atlas constructed by q-space diffeomorphic reconstruction. *NeuroImage*. 2011;58(1):91-99.

40. Yeh FC, Wedeen VJ, Tseng WYI. Generalized q-sampling imaging. *IEEE transactions on medical imaging*. 2010;29(9):1626-1635.

41. Yeh FC, Liu L, Hitchens TK, Wu YL. Mapping immune cell infiltration using restricted diffusion MRI. *Magnetic resonance in medicine*. 2017;77(2):603-612.

42. Yeh FC, Verstynen TD, Wang Y, Fernández-Miranda JC, Tseng WYI. Deterministic diffusion fiber tracking improved by quantitative anisotropy. *PloS One*. 2013:vol. 8, no. 11.

43. Folch-Fortuny A, Arteaga F, Ferrer A. Missing data imputation toolbox for MATLAB. *Chemometrics and Intelligent Laboratory Systems*. 2016;154:93-100.

44. Gibbons LE, Carle AC, Scott-Mackin R, et al. Composite measures of executive function and memory: ADNI_EF and ADNI_Mem. October 23, 2015. Accessed May 2021.

45. Choi SE, Mukherjee S, Gibbons LE, et al. Development and validation of language and visuospatial composite scores in ADNI. *Alzheimer's & Dementia: Translational Research & Clinical Interventions*. 2020;6(1):e12072.

46. Alzheimer's Disease Neuroimaging Initiative. ADNI2 Procedures Manual. July 2008. https://adni.loni.usc.edu/wp-content/uploads/2008/07/adni2-procedures-manual.pdf. Accessed May 2021.

47. Iturria-Medina Y, Carbonell FM, Assadi A, et al. NeuroPM toolbox: integrating Molecular, Neuroimaging and Clinical data for Characterizing Neuropathological Progression and

Individual Therapeutic Needs. *medRvix DOI: 10.1101/2020.09.24.20200964*. 2020.

48. Honey CJ, Sporns O, Cammoun L, et al. Predicting human resting-state functional connectivity from structural connectivity. *Proceedings of the National Academy of Sciences*. 2009;106(6):2035-2040.

49. Desikan R, Fan C, Wang Y, et al. Genetic assessment of age-associated Alzheimer disease risk: Development and validation of a polygenic hazard score. *PLoS medicine*. March 2017;14(3):e1002258.

50. Wu JW, Hussaini SA, Bastille IM, et al. Neuronal activity enhances tau propagation and tau pathology in vivo. *Nature neuroscience*. 2016;19(8):1085-10.

51. Zhang F, Gannon M, Chen Y, et al. β-amyloid redirects norepinephrine signaling to activate the pathogenic GSK3β/tau cascade. *Science Translational Medicine*. 2020;12(526).

52. Wang YJ, Ren QG, Gong WG, et al. Escitalopram attenuates β-amyloid-induced tau hyperphosphorylation in primary hippocampal neurons through the 5-HT1A receptor mediated Akt/GSK-3β pathway. *Oncotarget*. 2016;7(12):13328.

53. Wang R, Reddy PH. Role of glutamate and nmda receptors in Alzheimer's disease. *Journal of Alzheimer's Disease*. 2017;57(4):1041-1048.

54. Hynd MR, Scott HL, Dodd PR. Glutamate-mediated excitotoxicity and neurodegeneration in Alzheimer's disease. *Neurochemistry international*. 2004;45(5):583-595.

55. Butterfield DA, Pocernich CB. The glutamatergic system and Alzheimer's disease. *CNS drugs*. 2003;17(9):641-652.

56. Xu Y, Yan J, Zhou P, et al. Neurotransmitter receptors and cognitive dysfunction in alzheimer's disease and parkinson's disease. *Progress in neurobiology*. 2012;97(1):1–13.

57. Lau CG, Zukin RS. NMDA receptor trafficking in synaptic plasticity and neuropsychiatric disorders. *Nature Reviews Neuroscience*. 2007;8(6):413-426.

58. Chang EH, Savage MJ, Flood DG, et al. AMPA receptor downscaling at the onset of Alzheimer's disease pathology in double knockin mice. *Proceedings of the National Academy of Sciences*. 2006;103(9):3410-3415.

59. Yasuda RP, Ikonomovic MD, Sheffield R, Rubin RT, Wolfe BB, Armstrong DM. Reduction of AMPA-selective glutamate receptor subunits in the entorhinal cortex of patients with Alzheimer's disease pathology: a biochemical study. *Brain research*. 1995;678(1-2):161-167.

60. Carter TL, Rissman RA, Mishizen-Eberz AJ, et al. Differential preservation of AMPA receptor subunits in the hippocampi of Alzheimer's disease patients according to Braak stage. *Experimental neurology*. 2004;187(2):299-309.

61. Miller EC, Teravskis PJ, Dummer BW, Zhao X, Huganir RL, Liao D. Tau phosphorylation and tau mislocalization mediate soluble Aβ oligomer-induced AMPA glutamate receptor signaling deficits. *European Journal of Neuroscience*. 2014;39(7):1214-1224.

62. Iadecola C. Neurovascular regulation in the normal brain and in Alzheimer's disease. *Nature Reviews Neuroscience*. 2004;5(5):347-360.

63. Bangen KJ, Clark AL, Edmonds EC, et al. Cerebral Blood Flow and Amyloid-β Interact to Affect Memory Performance in Cognitively Normal Older Adults. *Frontiers in Aging Neuroscience*. 2017;9:181.

64. Bryant AG, Hu M, Carlyle BC, et al. Cerebrovascular Senescence Is Associated With Tau Pathology in Alzheimer's Disease. *Frontiers in neurology*. 2020;11:1058.

65. Ittner LM, Götz J. Amyloid-β and tau—a toxic pas de deux in alzheimer's disease. *Nature Reviews Neuroscience*. 2011;12(2): 67–72.

66. Bischof GN, Jessen F, Fliessbach, et al. Impact of tau and amyloid burden on glucose metabolism in Alzheimer's disease. *Annals of clinical and translational neurology*. 2016;3(12):934-939.

67. Planel E, Miyasaka T, Launey T, et al. Alterations in glucose metabolism induce hypothermia leading to tau hyperphosphorylation through differential inhibition of kinase and phosphatase activities: implications for Alzheimer's disease. *Journal of Neuroscience*. 2004;24(10):2401-2411.

68. Menkes-Caspi N, Yamin HG, Kellner V, Spires-Jones TL, Cohen D, Stern EA. Pathological tau disrupts ongoing network activity. *Neuron*. 2015;85(5):959-966.

69. Verma S, Kumar A, Tripathi T, Kumar A. Muscarinic and nicotinic acetylcholine receptor agonists: current scenario in Alzheimer's disease therapy. *Journal of Pharmacy and Pharmacology*. 2018.;70(8):985-993.

70. Hampel H, M-M M, Cuello AC, et al. Revisiting the cholinergic hypothesis in alzheimer's disease: Emerging evidence from translational and clinical research. *Alzheimer's Dementia*. 2017;6(1):2-15.

71. Grothe M, Zaborszky L, Atienza M, et al. Reduction of basal forebrain cholinergic system parallels cognitive impairment in patients at high risk of developing Alzheimer's disease. *Cerebral Cortex*. 2010;20(7):1685-1695.

72. Li Y, Sun H, Chen Z, Xu H, Bu G, Zheng H. Implications of GABAergic neurotransmission

in Alzheimer's disease. *Frontiers in aging neuroscience*. 2016;8:31.

73. Levenga J, Krishnamurthy P, Rajamohamedsait H, et al. Tau pathology induces loss of GABAergic interneurons leading to altered synaptic plasticity and behavioral impairments. *Acta neuropathologica communiucations*. 2013;1(1):34.

74. Limon A, Reyes-Ruiz JM, Miledi R. Loss of functional GABAA receptors in the Alzheimer diseased brain. *Proceedings of the National Academy of Sciences*. 2012;109(25):10071-10076.

75. Whittington RA, Virág L, Gratuze M, et al. Administration of the benzodiazepine midazolam increases tau phosphorylation in the mouse brain. *Neurobiology of aging*. 2019;75:11-24.

76. Küblböck M, Woletz M, Höflich A, et al. Stability of low-frequency fluctuation amplitudes in prolonged resting-state fMRI. *Neuroimage*. December 2014;1(103):249-257.

77. Zuo XN, Xing XX. Test-retest reliabilities of resting-state FMRI measurements in human brain functional connectomics: a systems neuroscience perspective. *Neuroscience & Biobehavioral Reviews*. September 2014;45:100-118.

78. Zang Y, Jiang T, Lu Y, He Y, Tian L. Regional homogeneity approach to fMRI data. *NeuroImage*. 2004;22(1):394-400.

79. Heuvel MPVD, Pol HEH. Exploring the brain network: a review on resting-state fMRI functional connectivity. *European neuropsychopharmacology*. 2010;20(8):519-534.

80. Lu H, Jaime S, Yang Y. Origins of the resting-state functional MRI signal: potential limitations of the "neurocentric" model. *Frontiers in neuroscience*. October 2019;13:1136.

81. Riedl V, Utz L, Castrillon G, et al. Metabolic connectivity mapping reveals effective connectivity in the resting human brain. *Proceedings of the National Academy of Sciences*. 2016;113(2):428-433.

82. Deco G, Ponce-Alvarez A, Mantini D, Romani GL, Hagmann P, Corbetta M. Resting-state functional connectivity emerges from structurally and dynamically shaped slow linear fluctuations. *Journal of Neuroscience*. 2013;33(27):11239-11252.

83. Bright MG, Whittaker JR, Driver ID, Murphy K. Vascular physiology drives functional brain networks. *NeuroImage*. 2020;217:116907.

84. Aso T, Sugihara G, Murai T, et al. A venous mechanism of ventriculomegaly shared between traumatic brain injury and normal ageing. *Brain*. June 2020;143(6):1843-1856.

85. Kaur S, DasGupta G, Singh S. Altered Neurochemistry in Alzheimer's Disease: Targeting Neurotransmitter Receptor Mechanisms and Therapeutic Strategy. *Neurophysiology*. 2019:1-17.

86. Whitehouse PJ, Au KS. Neurotransmitter receptor alterations in Alzheimer's disease. *Senile Dementia of the Alzheimer Type*. 1985:175-182.

87. Bishop NA, Lu T, Yankner BA. Neural mechanisms of ageing and cognitive decline. *Nature*. 2010;464(7288):529–535.

88. Guntupalli S, Widagdo J, Anggono V. Amyloid-β-induced dysregulation of AMPA receptor trafficking. *Neural plasticity*. 2016;2016.

89. Maes C, Hermans L, Pauwels L, et al. Age-related differences in GABA levels are driven by bulk tissue changes. *Human Brain Mapping*. 2018;39(9):3652-3662.

90. Nasrallah FA, Griffin JL, Balcar VJ, Rae C. Understanding your inhibitions: modulation of brain cortical metabolism by GABAB receptors. *Journal of Cerebral Blood Flow & Metabolism*. 2007;27(8):1510-1520.

91. Pavia J, De Ceballos ML, De La Cuesta FS. Alzheimer's disease: relationship between muscarinic cholinergic receptors, β-amyloid and tau proteins. *Fundamental & clinical pharmacology*. 1998;12(5):473-481.

92. Petersen RC, Aisen PS, Beckett LA, et al. Alzheimer's disease neuroimaging initiative (ADNI): Clinical characterization. *Neurology*. 2010;74(3):201–209.

93. Yeh FC, Verstynen TD, Wang Y, Fernández-Miranda JC, Tseng WYI. Deterministic diffusion fiber tracking improved by quantitative anisotropy. *PloS One*. 2013;8(11):e80713.

Supplementary Table S1*: Summary of demographic data for subjects included in 3 analysis: i) all re-MCM models, ii) healthy subjects that did not progress to MCI or AD, and iii) subjects that developed AD.*

Category	**All re-MCM subjects**	**Healthy Aging**	**AD**
Total subjects	423	112	25
Female	194 (45.9%)	56 (50.0%)	9 (36.0%)
Mean age (years)	71.8 (±7.0)	73.8 (±6.0)	72.0 (±5.5)
Mean education (years)	16.4 (±2.7)	16.5 (±2.8)	16.4 (±2.8)
APOE4 positive	175 (41.4%)	35 (31.2%)	8 (32.0%)

Supplementary Table S2: *Proportion of subjects with multi-modal neuroimaging data by clinical subgroup.*

Category	**All re-MCM subjects**	**Healthy Ageing**	**AD**
CBF	195 (46.1%)	39 (34.8%)	16 (64.0%)
Amyloid	422 (99.8%)	112 (100.0%)	25 (100.0%)
Neural Activity	127 (30.0%)	32 (28.6%)	6 (24.0%)
Metabolism	418 (98.8%)	109 (97.3%)	24 (96.0%)
Gray Matter	423 (100.0%)	112 (100.0%)	25 (100.0%)
Tau	238 (56.3%)	82 (73.2%)	14 (56.0%)

Supplementary Table S3: *Neurotransmitter receptor ligands used to obtain receptor maps.*

Neurotransmitter	Receptor	Ligand	Type
Glutamate	AMPA	[^{3}H]-AMPA	Agonist
	NMDA	[^{3}H]-MK-801	Antagonist
	Kainate	[^{3}H]-Kainate	Agonist
GABA	$GABA_A$	[^{3}H]-Muscimol	Agonist
	$GABA_B$	[^{3}H]-CGP 54626	Antagonist
	$GABA_A$-associated benzodiazepine binding site ($GABA_A$/BZ)	[^{3}H]-Flumazenil	Antagonist
Acetylcholine	M_1	[^{3}H]-Pirenzepine	Antagonist
	M_2	[^{3}H]-Oxotremorine-M	Agonist
	M_3	[^{3}H]-4-DAMP	Antagonist
	Nicotinic $\alpha_4\beta_2$	[^{3}H]-Epibatidine	Agonist
Noradrenaline	α_1	[^{3}H]-Prazosin	Antagonist
	α_2	[^{3}H]-RX 821002	Antagonist
Serotonin	5-HT_{1A}	[^{3}H]-8-OH-DPAT	Agonist
	5-HT_2	[^{3}H]-Ketanserin	Antagonist
Dopamine	D_1	[^{3}H]-SCH 23390	Antagonist

Supplementary Table S4: *Jülich histological atlas regions. Note that regions are defined by cytoarchitecture, and thus do not correspond perfectly with functional regions.*

Lobe	Anatomical subdivision	Jülich area	Region name
Occipital lobe	Visual cortex	hOc1	Brodmann's area 17 / V1
		hOc2	Brodmann's area 18 / V2
		hOc4d	V4
		hOc3d	V3d
		hOc3v	V3v
		hOc4v	V4
	Extrastriate cortex	FG1	Part of Brodmann area 19
		FG2	Part of Brodmann area 19
Parietal lobe	Somatosensory cortex	1	Brodmann's area 1
		2	Brodmann's area 2
		3a	Brodmann's area 3a
		3b	Brodmann's area 3b
	Superior parietal lobule	5L	Brodmann's area 5L
		5M	Brodmann's area 5M
		7A	Brodmann's area 7A
	Inferior parietal lobule	PGa	Anterior inferior parietal area
		PGp	Posterior inferior parietal area
		PFt	Temporal inferior parietal area
		PFm	Medial inferior parietal area
Temporal lobe	Auditory cortex	Te1	Temporal area 1 (part of Brodmann's area 41)
		Te2	Temporal area 2 (part of Brodmann's area 41)
	Hippocampus	CA+dentate	Cornu ammonis + fascia dentata
	Entorhinal cortex	Ent	Brodmann's area 28

		20	Brodmann's area 20
		21	Brodmann's area 21
		22	Brodmann's area 22
		36	Brodmann's area 36
		37	Brodmann's area 37
		38	Brodmann's area 38
Frontal lobe	Agranular premotor cortex	6	Brodmann's area 6
	Primary motor cortex	4p	Brodmann's area 4p
	Broca's region	44	
		45	
	Frontopolar cortex	Fp1	Frontopolar area (part of Brodmann area 10)
		Fp2	Frontopolar area (part of Brodmann area 10)
	Orbitofrontal cortex	Fo1	Orbitofrontal area (part of Brodmann area 11)
	Lateral prefrontal	46	Brodmann's area 46
		47	Brodmann's area 47
		8	Brodmann's area 8
		9	Brodmann's area 9
Cingulate regions (multiple lobes)	Anterior cingulate	p24ab	Pregenual cingulate areas p24a & p24b
		p32	Pregenual cingulate area p32
	Posterior cingulate	23	Brodmann's area 23
		31	Brodmann's area 31

Supplementary Table S5: *Biological parameters most correlated with cognitive decline in AD, and the percentage of cognitive decline variance explained.*

Neuroimaging Modality	Model Parameter	Receptor Type	Explained Variance
CBF	NMDA × CBF	Glutamatergic	0.22%
	M_2 × CBF	Cholinergic	0.30%
	M_2 × Amyloid	Cholinergic	0.17%
	M_1	Cholinergic	0.30%
	α_1 × Gray Matter	Adrenergic	0.11%
	D_1 × Amyloid	Dopaminergic	0.22%
Amyloid	Kainate × CBF	Glutamatergic	0.10%
	AMPA × Tau	Glutamatergic	0.15%
	NMDA × Tau	Glutamatergic	0.18%
	Kainate × Tau	Glutamatergic	0.10%
	AMPA	Glutamatergic	0.13%
	$GABA_A$/BZ × CBF	GABAergic	0.33%
	$GABA_A$/BZ × Neural Activity	GABAergic	0.26%
	$GABA_A$/BZ × Metabolism	GABAergic	0.26%
	$GABA_A$/BZ × Tau	GABAergic	0.22%
	$GABA_B$	GABAergic	0.29%
	$\alpha_4\beta_2$	Cholinergic	0.29%
	α_2 × Amyloid	Adrenergic	0.19%
	α_2 × Tau	Adrenergic	0.11%
	α_2	Adrenergic	0.31%
	$5HT_2$ × CBF	Serotonergic	0.34%
	$5HT_{1A}$	Serotonergic	0.13%
	D_1 × Metabolism	Dopaminergic	0.15%
	Neural Activity	Non-Receptor	0.04%
	spreading	Non-Receptor	0.14%
Neural Activity	AMPA × CBF	Glutamatergic	0.24%
	Kainate × CBF	Glutamatergic	0.15%
	AMPA × Amyloid	Glutamatergic	0.16%
	AMPA × Neural Activity	Glutamatergic	0.14%
	AMPA × Metabolism	Glutamatergic	0.36%
	NMDA × Metabolism	Glutamatergic	0.15%
	AMPA × Gray Matter	Glutamatergic	0.42%
	AMPA × Tau	Glutamatergic	0.29%
	NMDA × Tau	Glutamatergic	0.30%
	Kainate × Tau	Glutamatergic	0.13%
	NMDA	Glutamatergic	0.15%
	$GABA_A$ × CBF	GABAergic	0.27%

	$GABA_B$ × CBF	GABAergic	0.35%
	$GABA_A$ × Gray Matter	GABAergic	0.23%
	$GABA_B$	GABAergic	0.27%
	M_1 × CBF	Cholinergic	0.11%
	M_2 × CBF	Cholinergic	0.17%
	M_2 × Amyloid	Cholinergic	0.16%
	M_3 × Neural Activity	Cholinergic	0.20%
	M_1 × Gray Matter	Cholinergic	0.14%
	M_2 × Gray Matter	Cholinergic	0.23%
	M_1	Cholinergic	0.12%
	M_3	Cholinergic	0.23%
	α_2 × CBF	Adrenergic	0.26%
	α_2 × Amyloid	Adrenergic	0.32%
	α_2 × Gray Matter	Adrenergic	0.15%
	$5HT_2$ × Gray Matter	Serotonergic	0.42%
	D_1 × Amyloid	Dopaminergic	0.29%
	D_1 × Gray Matter	Dopaminergic	0.49%
	D_1	Dopaminergic	0.31%
Metabolism	Kainate × Metabolism	Glutamatergic	0.11%
	Kainate × Tau	Glutamatergic	0.18%
	Kainate	Glutamatergic	0.14%
	$GABA_A$ × Tau	GABAergic	0.20%
	$GABA_A$/BZ × Tau	GABAergic	0.22%
	$\alpha_4\beta_2$ × CBF	Cholinergic	0.11%
	M_2 × Tau	Cholinergic	0.16%
	$\alpha_4\beta_2$ × Tau	Cholinergic	0.11%
	α_2 × Gray Matter	Adrenergic	0.11%
	α_1 × Tau	Adrenergic	0.14%
	$5HT_{1A}$ × Tau	Serotonergic	0.14%
	D_1 × Neural Activity	Dopaminergic	0.17%
	spreading	Non-Receptor	0.16%
Gray Matter	NMDA × Gray Matter	Glutamatergic	0.07%
	$GABA_A$/BZ × CBF	GABAergic	0.28%
	M_3 × CBF	Cholinergic	0.21%
	M_2 × Gray Matter	Cholinergic	0.10%
	α_2 × Metabolism	Adrenergic	0.07%
	$5HT_2$ × CBF	Serotonergic	0.18%
Tau	NMDA × CBF	Glutamatergic	0.16%
	Kainate × Amyloid	Glutamatergic	0.10%
	Kainate × Metabolism	Glutamatergic	0.36%
	$GABA_A$/BZ × CBF	GABAergic	0.29%

	$GABA_A$	GABAergic	0.12%
	$GABA_B$	GABAergic	0.27%
	M_3 × CBF	Cholinergic	0.33%
	$\alpha_4\beta_2$ × Amyloid	Cholinergic	0.17%
	M_2 × Neural Activity	Cholinergic	0.10%
	$\alpha_4\beta_2$ × Metabolism	Cholinergic	0.18%
	$\alpha_4\beta_2$ × Tau	Cholinergic	0.25%
	$\alpha_4\beta_2$	Cholinergic	0.36%
	α_1 × CBF	Adrenergic	0.12%
	α_1 × Metabolism	Adrenergic	0.11%
	α_2 × Metabolism	Adrenergic	0.24%
	α_2 × Gray Matter	Adrenergic	0.10%
	$5HT_2$ × CBF	Serotonergic	0.40%
	$5HT_{1A}$ × Amyloid	Serotonergic	0.15%
	$5HT_{1A}$ × Tau	Serotonergic	0.20%
	Metabolism	Non-Receptor	0.08%
	Gray Matter	Non-Receptor	0.25%

Supplementary Table S6: *Total cognitive variance explained by receptor type in AD patients (via the significant SVD component).*

Receptor Type	**Total Variance Explained**
Glutamatergic	4.47%
GABAergic	3.85%
Cholinergic	4.46%
Adrenergic	2.34%
Serotonergic	1.96%
Dopaminergic	1.63%

Supplementary Table S7: *Performance gain due to the inclusion of receptor maps, and the p-value from a two-sample t-test for each modality.*

Imaging Modality	**Average Gain in R^2**	**P-value**
CBF	125% ± 123%	P<0.001
Amyloid	119% ± 141%	P<0.001
Neural Activity	123% ± 150%	P<0.001
Metabolism	133% ± 200%	P<0.001
Gray Matter	234% ± 389%	P<0.001
Tau	141% ± 142%	P<0.001

Supplementary Table S8: *Performance gain due to true receptor distributions over null maps, and p-value of the true receptor data model belonging to the null distribution.*

Imaging Modality	Average Gain in R^2	P-value
CBF	19.5% ± 13.7%	P<0.01
Amyloid	20.5% ±15.3%	P<0.01
Neural Activity	22.3% ± 15.0%	P<0.01
Metabolism	15.6% ± 13.3%	P<0.04
Gray Matter	20.2% ± 18.4%	P<0.03
Tau	21.5% ± 13.0%	P<0.01

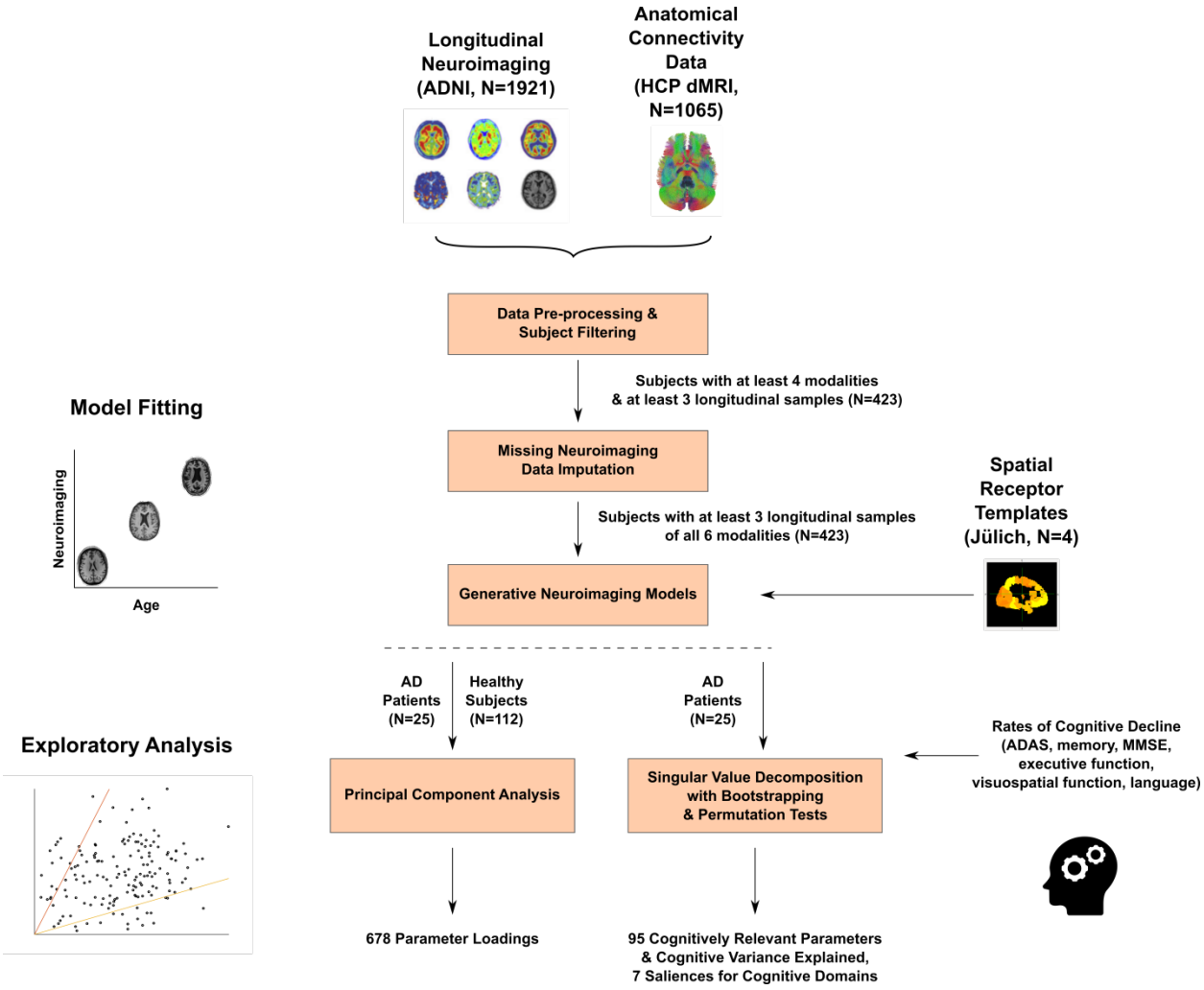

Supplementary Figure S1*: Modeling and analysis pipeline***.** First, multi-modal neuroimaging data, neurotransmitter receptor maps and tractography-derived connectivity matrices are used to fit personalized neuroimaging models. PCA was used to identify biological parameters contributing to inter-individual variability in healthy and AD subgroups. Subsequently, model parameters were compared to the subject-wise variation of cognitive decline in the AD subgroup using singular value decomposition. SVD allows the ranking of parameters based on the variance explained, allowing the identification of prominent alterations.

a) Data variance explained by restricted model without receptor-imaging interactions

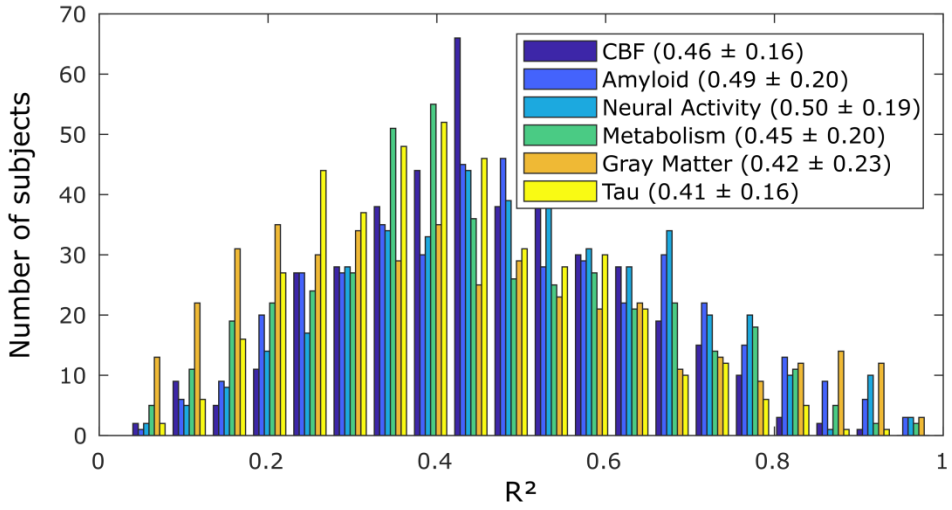

b) Proportion of individual models significantly improved by including only direct receptor terms

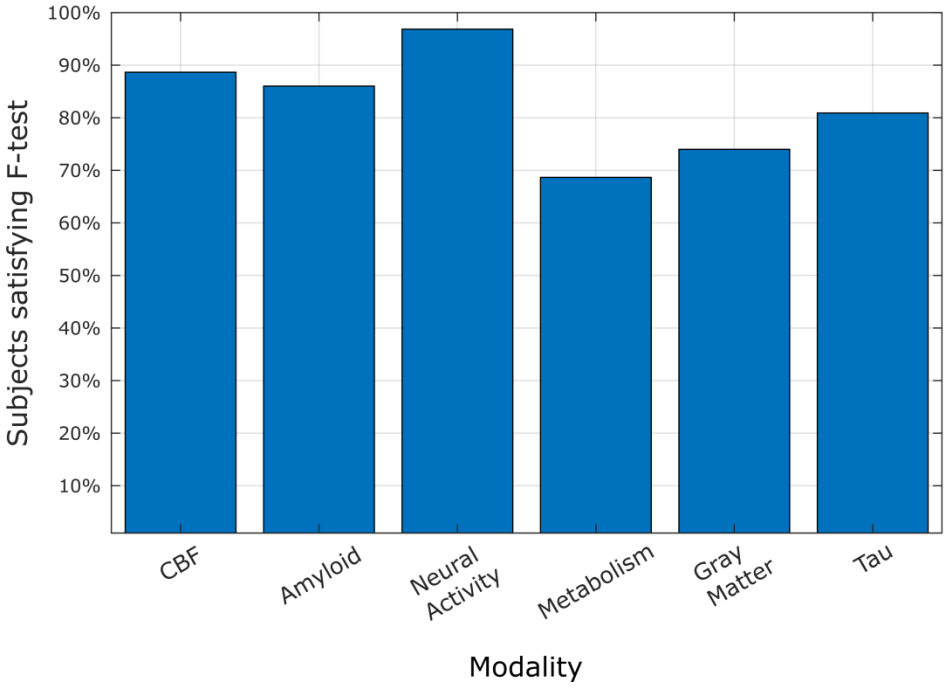

Supplementary Figure S2: *Receptor maps improve neuroimaging model accuracy.* In all (N=423) subjects, we fit personalized neuroimaging models using receptor maps and neuroimaging data, but excluding receptor-neuroimaging interactions. a) The distribution of R^2 shows a moderate improvement over the restricted model with no receptor data (Fig. 2b). b) The majority of subjects showed a significant ($P<0.05$) improvement in R^2, based on an F-test between the restricted, interaction-free model (with receptor maps) and the neuroimaging-only model of Fig. 2b.

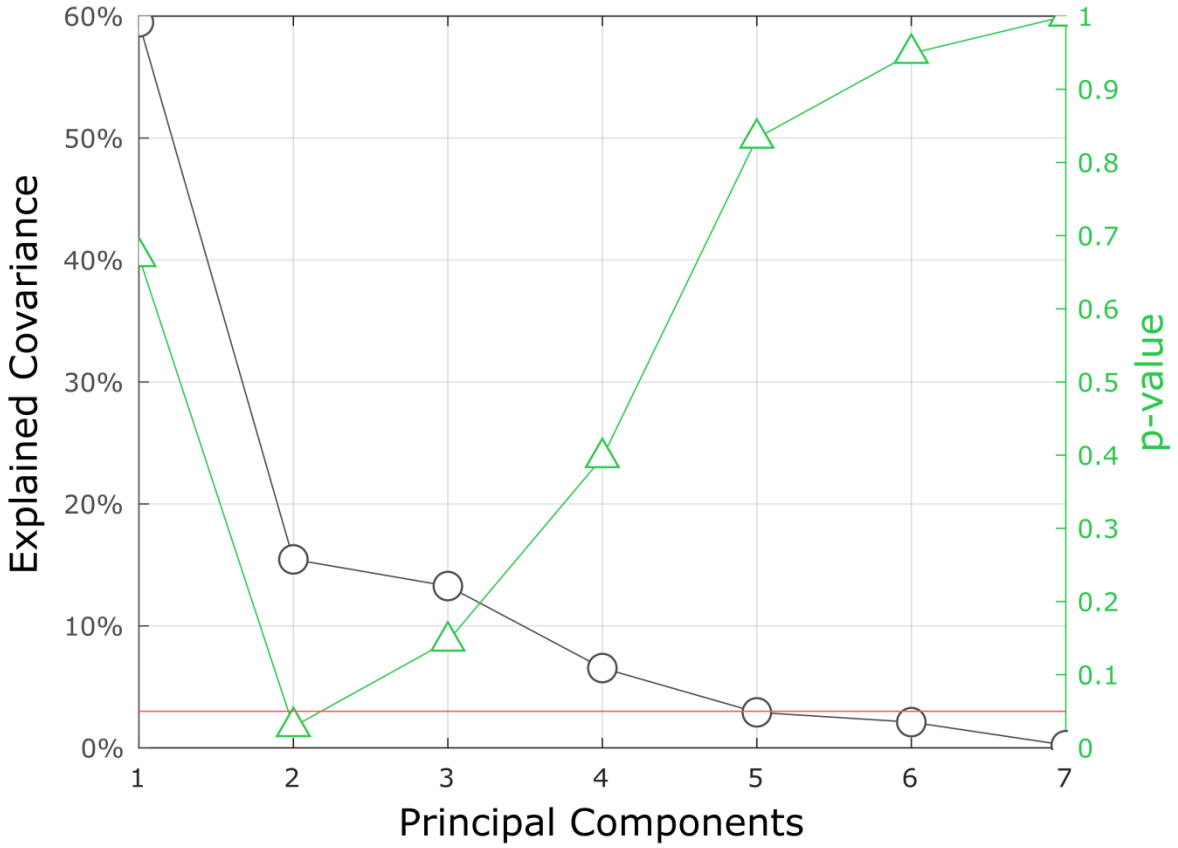

Supplementary Figure S3: *Secondary significant component links biological parameters to cognitive decline in healthy ageing*. We performed singular value decomposition linking biological parameters to rates of cognitive decline in N=112 healthy subjects. The latent components are ranked by the fraction of cognitive decline variance explained, and p-value based on the permutation analysis outlined in *Biological parameter cognitive significance analysis.* A minor SVD component linking re-MCM parameters to rates of cognitive decline was significant ($p<0.02$ for the second component).

Supplementary Figure S4: *Significant neurotransmitter receptor-imaging interactions underlying cognitive decline in healthy aging (PC2;* 15.5% variance explained, p<0.02; *N=112).* Receptor-imaging interactions significantly correlated, via the second principal component, to cognitive decline in healthy aging are shown.

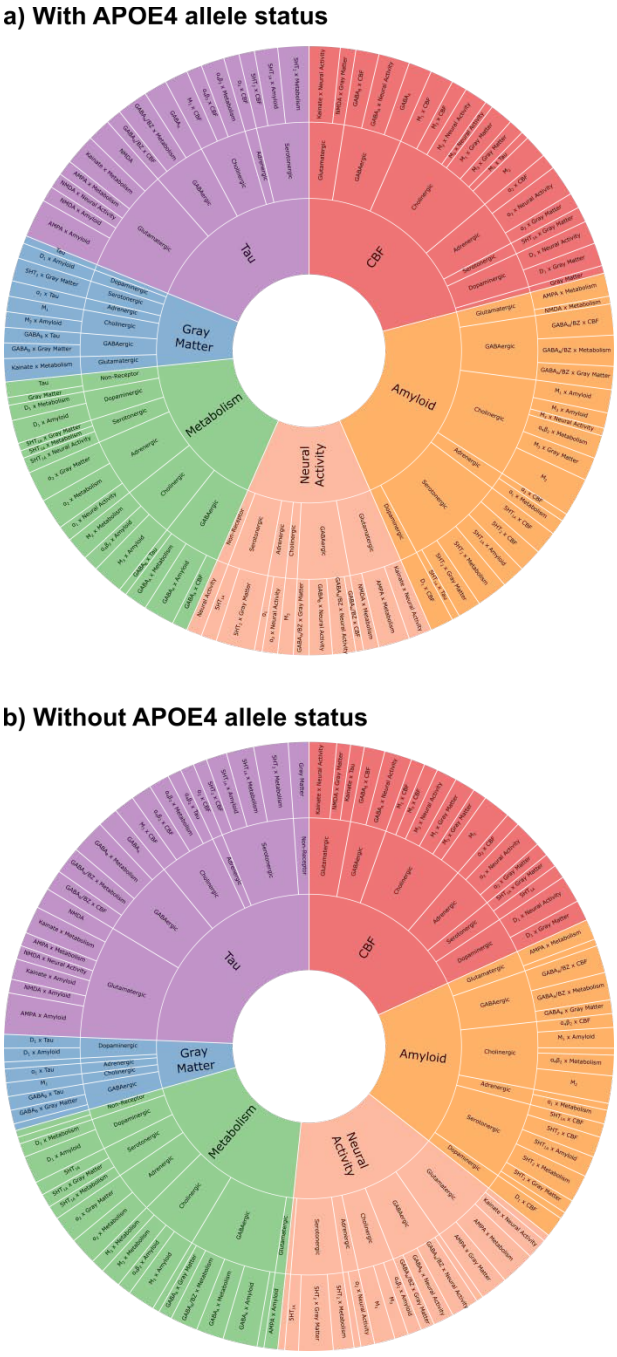

Supplementary Figure S5: *Effect of APOE4 status on significant neurotransmitter receptor-imaging interactions underlying cognitive decline in MCI and AD subjects (N=177).* a) Cognitive decline variance explained by significant receptor-imaging interactions identified after covariate adjustment of subjects' model parameters by APOE ε4 allele status, for the first principal component (40.2% variance explained, $p<0.001$). b) Significant interactions identified without covariate adjustment by APOE status in the same subgroup, for the first principal component (41.9% variance explained, $p<0.001$).

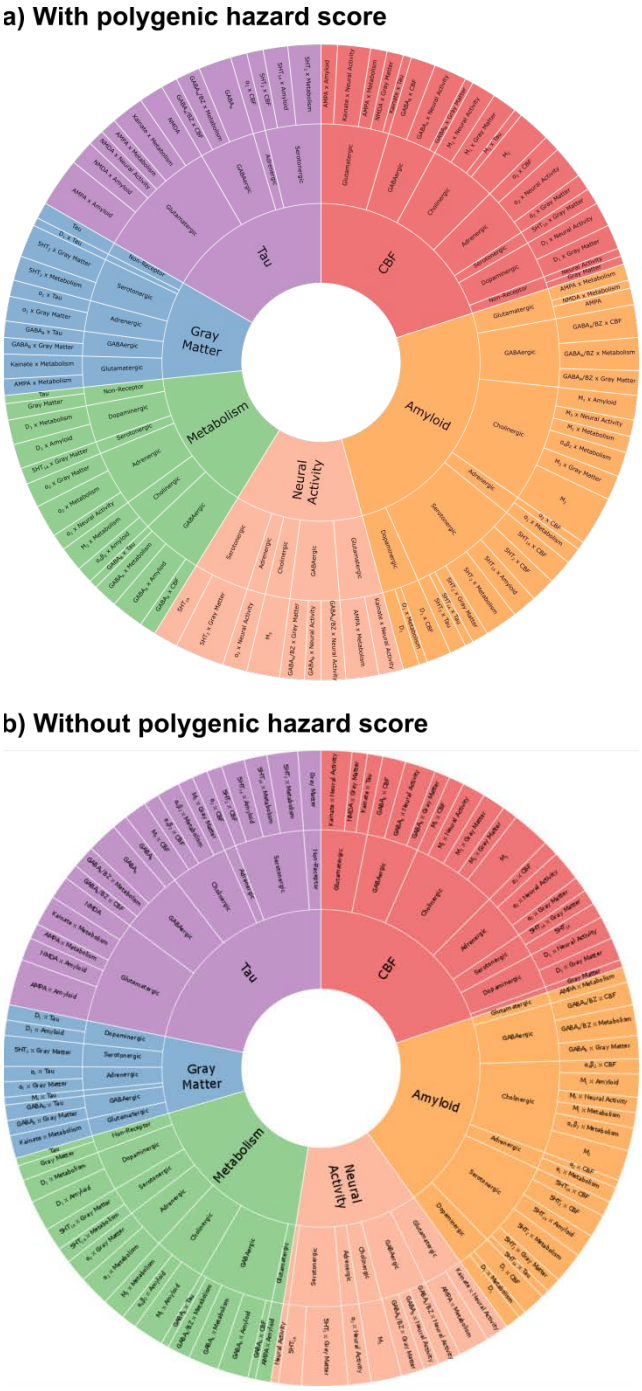

Supplementary Figure S6: *Effect of polygenic hazard score (PHS) on significant neurotransmitter receptor-imaging interactions underlying cognitive decline in MCI and AD subjects (N=161).* a) Cognitive decline variance explained by receptor-imaging interactions identified after covariate adjustment of subjects' model parameters by polygenic hazard scores, for the first principal component (40.6% variance explained, $p<0.001$). b) Significant interactions identified without covariate adjustment by polygenic hazard score in the same subgroup, for the first principal component (42.2% variance explained, $p<0.001$).

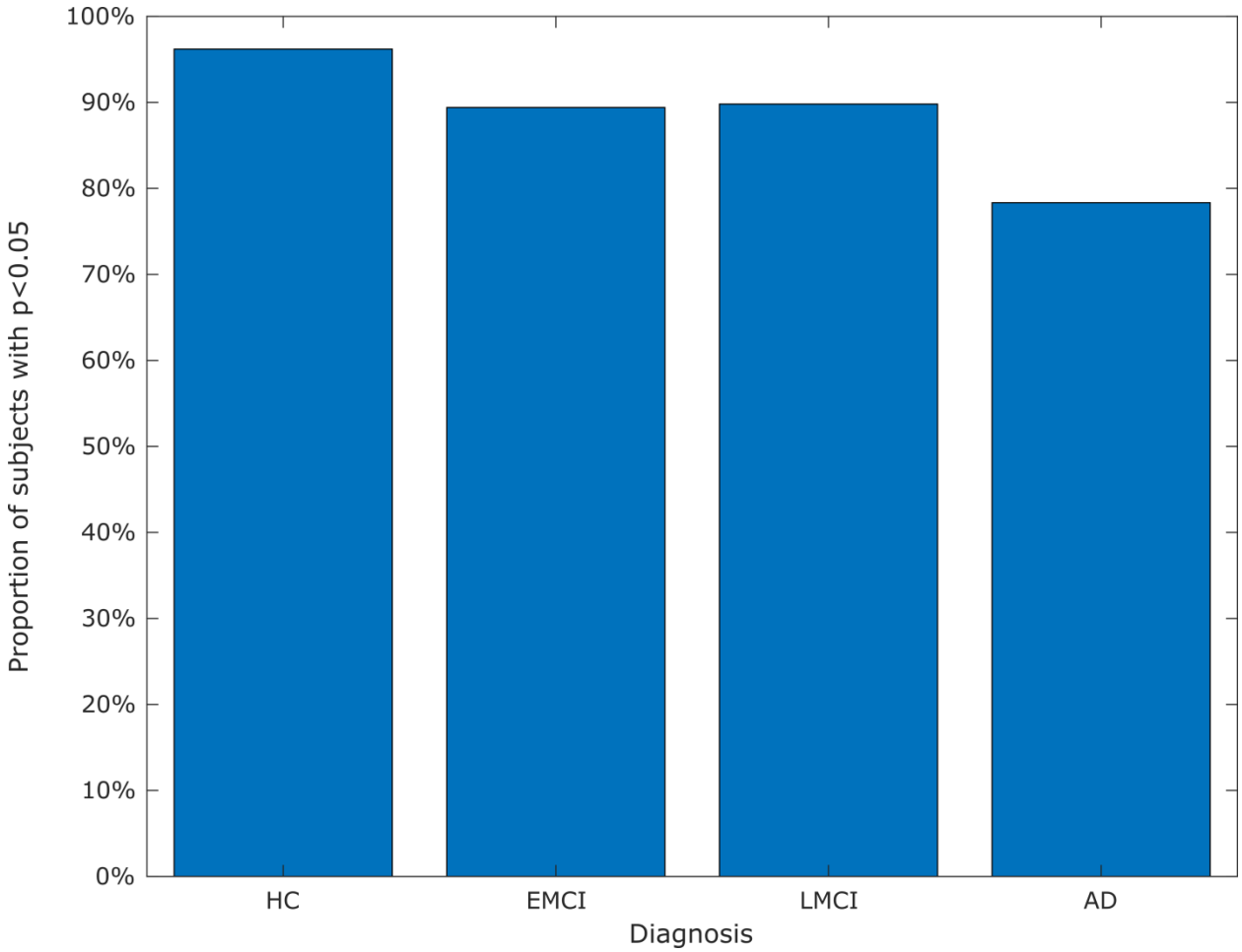

Supplementary Figure S7: *Distribution of significantly improved receptor template model fit by diagnoses (N=423).* The average number of subjects (across all 6 modalities) for whom the true receptor maps resulted in significantly better model fit ($p<0.05$) than the randomly permuted receptor maps. The receptor template is most informative for healthy subjects, and progressively less for MCI and AD subjects.

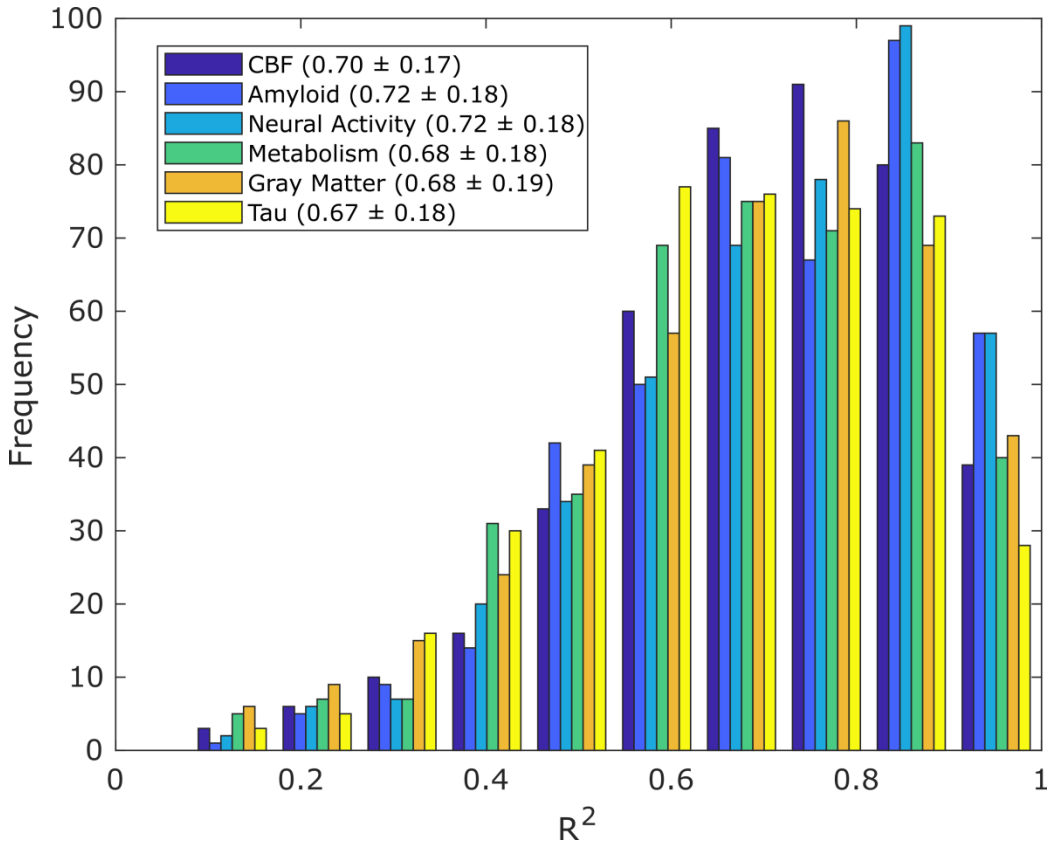

Supplementary Figure S8: *Distribution of model fit (R^2) for re-MCM models using functional connectivity (N=423).* The model performance is virtually indistinguishable from the structural connectivity model (Fig. 2; r>0.99 for all modalities).

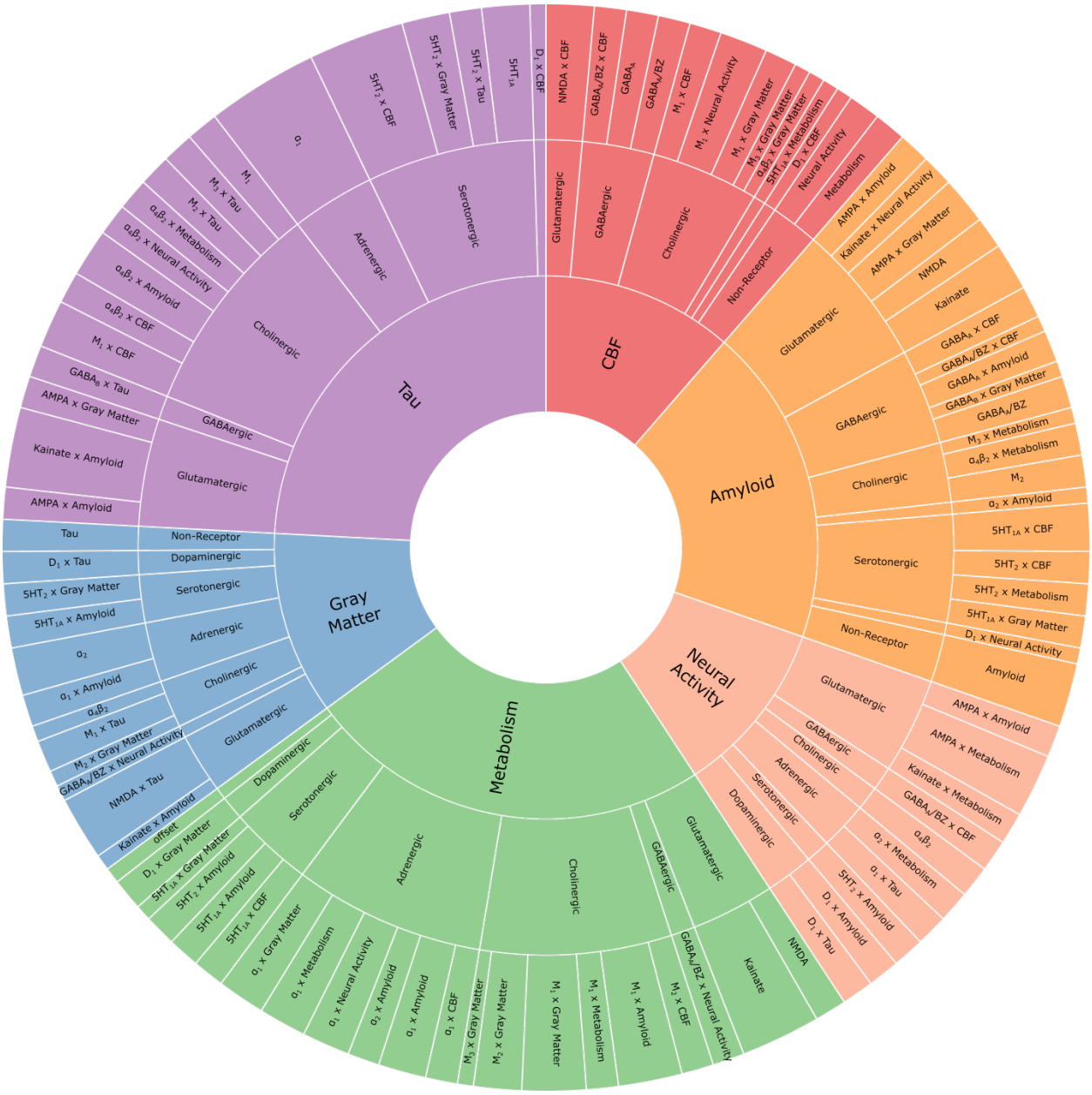

Supplementary Figure S9: *Model parameters significant to cognitive decline in amyloid-positive MCI and AD subjects (N=52).* Cognitive decline variance explained by receptor-imaging interactions, for the first principal component (44.3% variance explained, $p<0.003$; $r=0.76$, $p<10^{-8}$ after removing outliers more than 3 MAD from the projections of model parameters and cognitive scores, $p<0.001$).

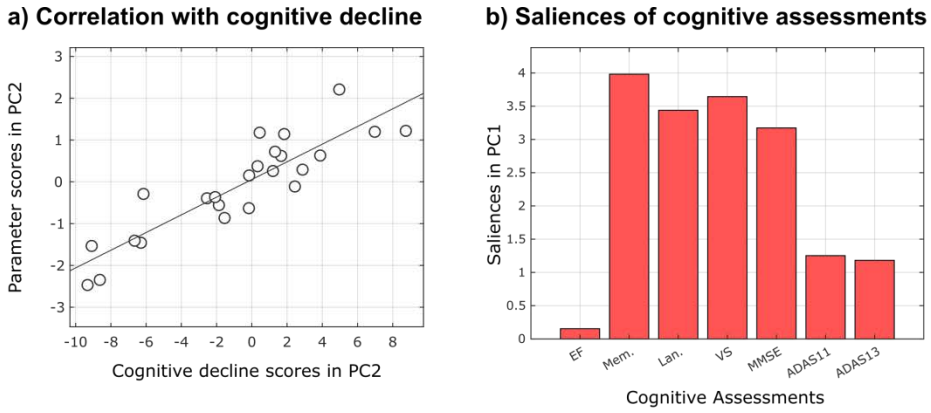

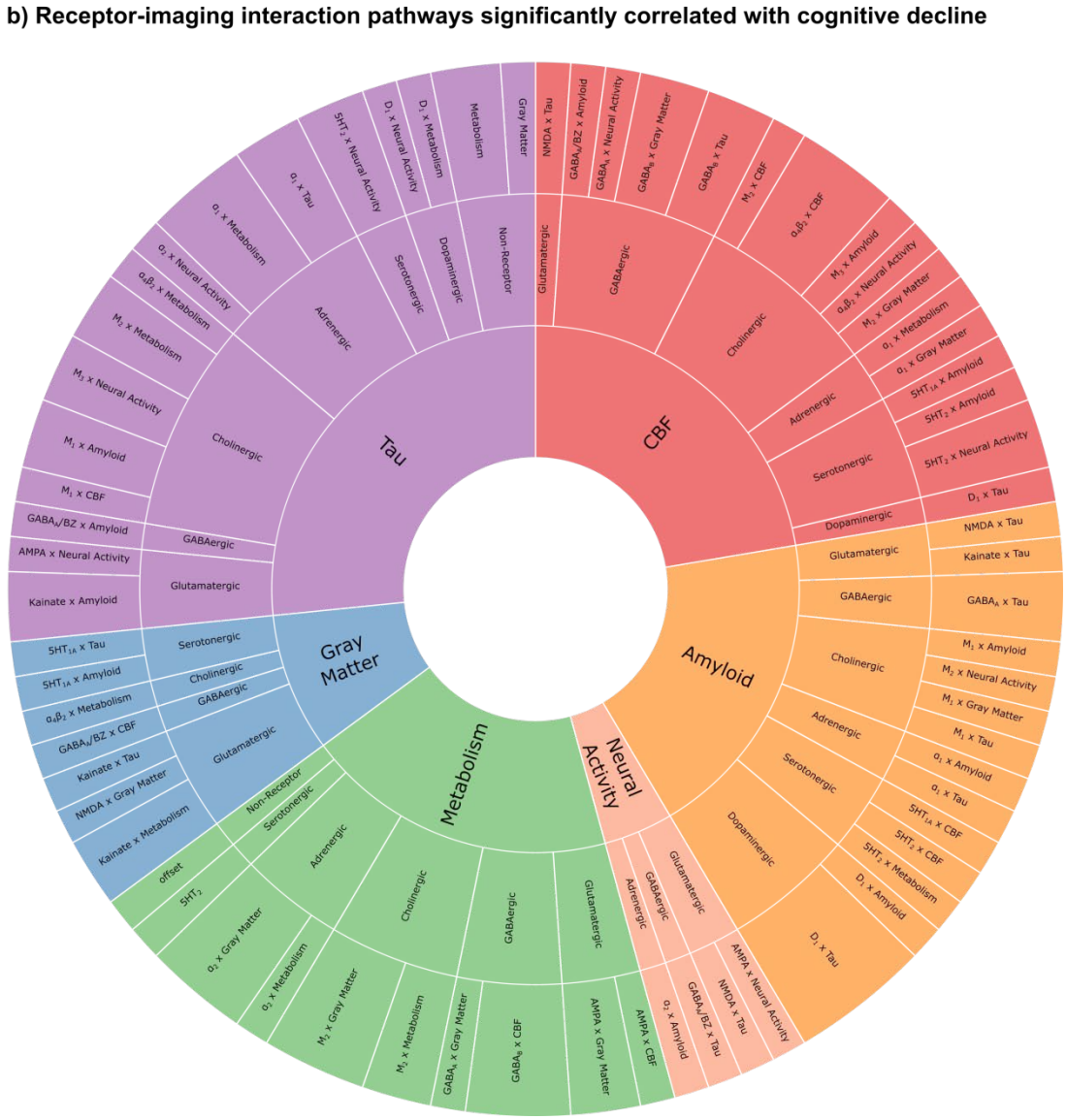

Supplementary Figure S10: *Second component of receptor-cognitive variance in AD (N=25).* Contributions of receptor-imaging interactions to explaining the inter-subject variance between model parameters and cognitive scores projected to the second principal component (23.4%

variance explained, $p<0.051$). a) The second component also showed a high correlation between model parameters and cognitive scores ($r=0.890$, $p<10^{-8}$). b) Cognitive variance in this axis showed a lower contribution of executive dysfunction. c) Receptor-imaging interactions in the second component showed a lower contribution due to neural activity model parameters, and a greater contribution due to CBF and metabolism models.